Finite Element Analysis of a Composite Sandwich Beam Subjected to a Four Point Bend

By

Darlington Hove

Submitted in fulfilment of the requirements for the degree of

Magister Scientiae

in the Faculty of Science at the

Nelson Mandela Metropolitan University

Supervisor: Prof. John W. Gonsalves

Co-Supervisor: Prof. Rajesh D. Anandjiwala

Date: January 2011

Abstract

The work in this dissertation deals with the global structural response and local damage effects of a simply supported natural fibre composite sandwich beam subjected to a four-point bend. For the global structural response, we are investigating the flexural behaviour of the composite sandwich beam. We begin by using the principle of virtual work to derive the linear and nonlinear Timoshenko beam theory. Based on these theories, we then proceed to develop the respective finite element models and then implement the numerical algorithm in MATLAB. Comparing the numerical results with experimental results from the CSIR, the numerical model correctly and qualitatively recovers the underlying mechanics with some noted deviances which are explained at the end.

The local damage effect of interest is delamination and we begin by reviewing delamination theory with more emphasis on the cohesive zone model. The cohesive zone model relates the traction at the interface to the relative displacement of the interface thereby creating a material model of the interface. We then carry out a cohesive zone model delamination case study in MSC.Marc and MSC.Mentat software packages. The delamination modelling is carried out purely as a numerical study as there are no experimental results to validate the numerical results.

Acknowledgments

I wish to express my sincere gratitude to my supervisor, Professor John Gonsalves for the guidance, encouragement and for making me feel at home from the first day of arrival in the Department, which started before I became an NMMU student. During my stay, a lot happened and I faced many setbacks and I thank him for standing by me during the whole time. More than anything, I thank him for those many hours he spent reviewing and proof reading various drafts of this dissertation. I would also like to give a special mention to my co-supervisor, Prof Rajesh Anandjiwala, for the kind support and assistance. I do appreciate the helpful discussions we had which helped to shape up this study. I would like to thank the following researchers who helped me by supplying me with their papers for my literature review: Professor Paul Lagace of Massachusetts Institute of Technology, Professor Marcelo F.S.F de Moura from the University of Porto and Professor Dave Reedy from Sandia Laboratories.

I would like to thank the Council for Scientific and Industrial Research in South Africa (CSIR) and the Department of Science and Technology (DST) for providing much needed financial assistance and availing lab facilities and materials which made this work possible. I also acknowledge the contribution by Dr. Maya John of CSIR for the guidance with experiments and experimental data. I would like to acknowledge the assistance I got with numerical simulations and access to

software from Mr. Clive Hands of NMMU Department of Mechanical Engineering. I am indebted to Dr. Vitalis Musara for the help during proof-reading of my document. I would like to express my utmost gratitude to the NMMU Research Capacity Department for the financial support in the form of the NMMU Post Graduate Research Scholarship. Special thanks also go to the NMMU Department of Mathematics and Applied Mathematics for their unwavering financial support as and whenever the need arose in the form of bursaries and various assistantships. To this end, I would like to single out Professor W. Olivier, Prof G. Booth, Prof Strauelli and Prof Gonsalves for the financial support during my times of need. I would to thank Prof A. Leitch and the Faculty of Science for the Faculty Bursary which helped cushion me.

I do acknowledge the love and support of my mother, my siblings Donald, Doreen Musalad, Tapiwa, Mako, Munashe and Ropafadzo. I also acknowledge the prayers I got from my churchmates in the Evangelical Lutheran Church in Zimbabwe, Glen view congregation. I say: The support I got from you guys was outstanding and you were there when I needed you most. I also thank the help and advise of friends and colleagues who in whatever way, contributed into the writing of this dissertation but have not been mentioned explicitly. Most of all, I would like to salute my mentor, hero, kind friend and father, Engineer Dominic Hove aka Victor Pasipanodya. I thank him for the financial sacrifice that allowed me to

commence my Masters studies and the wise words of wisdom and encouragement. Though he passed away during the course of my studies, I am glad I have achieved because of him. Words are not enough and I say, rest in peace.

Port Elizabeth, South Africa Darlington Hove

06 January 2011

Contents

List of Figures

Chapter 1
Introduction

1.1 Background

The use of sandwich structures in industry is ever on the rise due to their high strength to weight ratio. A typical sandwich panel consists of a light core material sandwiched between two thin composite facings [JOHNSON and HOLZAPFEL, 2003]. The core of a composite sandwich panel is made from either honeycomb paper or foam whilst the facesheets are made of carbon fibre reinforced plastic. The sandwich panel construction answered the aerospace industry's need for an efficient shell structure by significantly increasing bending stiffness for a minimal increase in weight. With its increased use, comes the need for an understanding of the failure mechanisms a composite sandwich structures undergo. The CSIR, in collaboration AIRBUS, developed a natural fibre based composite sandwich beam for use in aircraft cabin interiors [ANANDJIWALA et al., 2008]. If successful, these natural fibre composite sandwich beams can unlock enormous environmental benefits since they are lightweight and biodegradable unlike the carbon fibre reinforced plastics which are generally not environmentally friendly. Another benefit is that since CSIR is manufacturing the natural fibre composite materials from crops grown in the Eastern Cape, the community stands to benefit directly through employment creation.

Whilst the automotive industry has successfully tried these natural fibre composite materials, their use in the aerospace industry demands these materials undergoing several

tests before finally passing the necessarily stringent safety regulations. Experiments can be performed to determine the failure mechanisms under different loading conditions, but carrying out experiments, whilst helpful in the initial characterisation of the failure modes, has its own limitations when failure under different sample sizes or loading conditions has to be analysed. Experiments are laborious, expensive and certainly time consuming, contributing to an increase in design time for new materials.

Instead of performing numerous experiments, we can resort to numerical techniques like the finite element method. The finite element method can be applied to beams of different shapes, sizes, material compositions, loadings and supports without the cost and time required for experimental testing [PALAZOTTO et al., 2000]. Another benefit of the finite element method is that it follows an orderly systematic approach that can be implemented easily on a digital computer [REDDY, 1993]. Commercial finite element packages are readily available and with extensive post processing capabilities, affording the analyst the flexibility to observe the solution from a variety of view points. The finite element method (FEM) has proved a useful tool in the analysis of structures. It has been used to analyse the response of composite sandwich panels to high velocity impact [BUITRAGO et al., 2010, HORRIGAN et al., 2000, IVANEZ et al., 2010], low velocity impact [PALAZOTTO et al., 2000, MEO et al., 2003, FOO et al., 2008] and also bending , which is a quasi-static response [CASTANIE et al., 2008, CHEN and BAI, 2002].

After an initial investigation into the combustion properties of the natural fibre composite sandwich panel [ANANDJIWALA et al., 2008], the CSIR has become more inter-

ested in its mechanical behaviour, strength and failure modes. This study will investigate two specific machanical problems: Firstly the flexural behaviour of a composite sandwich beam subjected to a four-point load will be investigated. Then, as the common failure modes of composite sandwich structures include fibre breakages, core crushing and core-facesheet delamination [LACY and HWANG, 2003] caused by mechanical defects, concentrated loads or impact. This study will attempt to model the delamination of the natural fibre composite structure.

Delamination, or interlaminar failure, is an important failure mode caused by interlaminar stresses. The composite sandwich panel begins to suffer delamination damage when the interlaminar stresses exceed the beam's interlaminar strength. Delamination can greatly reduce the structural integrity of a composite sandwich panel and alter its load carrying ability. The capture and control of any delamination onset requires accurate modelling and different methods have been used by researchers in the modelling of delamination [MEO and THIEULOT, 2005, WIMMER et al., 2009]. Delamination simulation consists of two stages, namely delamination initiation and delamination growth. Delamination initiation typically relies on stress based failure techniques whereas delamination growth relies on fracture mechanics techniques.

Fracture mechanics defines the amount of energy released per unit area during crack formation as the strain energy release rate [LUO and TONG, 2009]. For a delamination to grow, the strain energy release rate has to exceed a given threshold crack property known as

the critical energy release rate. The critical strain energy release rate is normally determined experimentally.

To model delamination propagation, the strain energy release rate is calculated and then compared with the given critical energy release rate with the delamination propagating only when the calculated energy release rate exceeds the critical energy release rate. A popular fracture mechanics approach used by researchers is the Virtual Crack Closure Technique (VCCT) developed by Rybocki and Kanninen (1997). The VCCT is based on Irwin's assumption, which states that the energy required to extend the length of a crack by a small amount is equal to the work done to close that crack back to its original length [KRUEGER, 2002, IRWIN, 1958]. The requirement of an initial crack in fracture mechanics approaches serves as a disadvantage for those situations in which a delamination can occur but without an initial crack [ZOU et al., 2003].

1.2 Composite Sandwich Beam Theory

A beam is a structure designed to resist transverse loads. In a beam, one side is significantly longer than the other two sides and we assume that the cross-sectional area of the beam remains constant throughout the length of the beam. The sandwich panel supplied by the CSIR for this study fits the definition of a beam and so it will be analysed as such. If the loading on the beam is a function of the longitudinal direction x only, then the beam bending problem can be solved as a one dimensional problem since the resulting displacements and stresses will also be functions of x only [REDDY, 2004]. In this study, we will

take the y direction as the width of the beam and the z direction as the height or thickness of the beam.

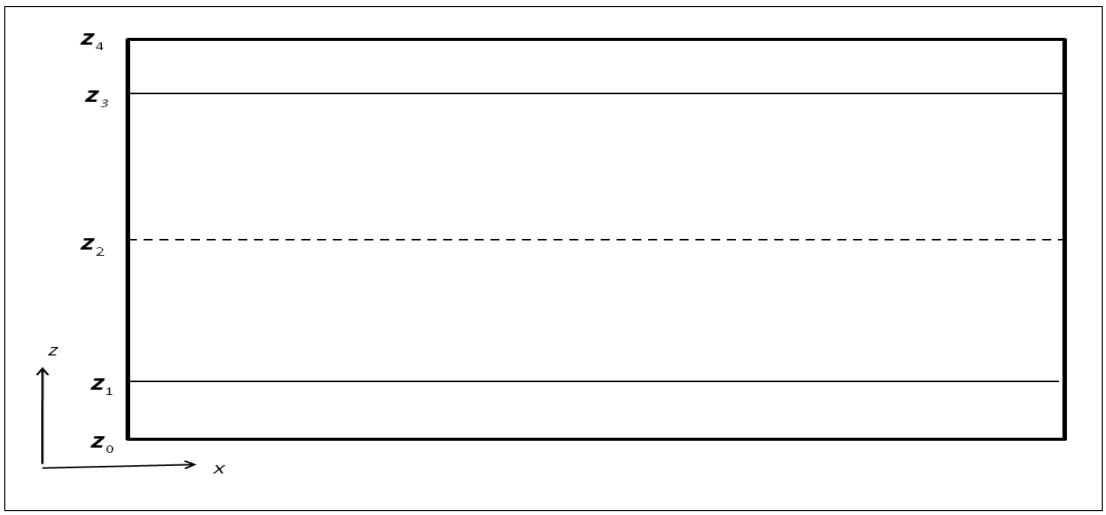

Fig. 1.1. Coordinate system and numbering used for a composite sandwich beam

The above Fig (1.1) gives a schematic view of a composite sandwich beam. The kth layer is located between the points $z = z_{k-1}$ and $z = z_k$ in the thickness direction. while the line $z = z_2 = 0$ denotes the midline. In order to analyse the panel as a symmetric composite beams, four layers have been created by conveniently placing the x-axis in the undeformed midline. The thin composite facings carry most of the bending stresses whilst the lightweight core absorbs most of the shear stresses giving rise to a structure with very high strength-weight ratio [GDOUTOS and DANIEL, 2008]

The simplest beam bending theory is the classical Euler-Bernoulli beam theory based on the following assumptions [REDDY, 2004]:

1. Transverse normals of the beam remain straight after deformation.

2. The length of the transverse normals remains unaltered after deformation.

3. The transverse normals remain perpendicular to the midline after deformation.

The third assumption necessarily implies that transverse shear strains are zero in the Euler-Bernoulli theory. This is generally valid for solid beams or very thin beams. Metals are generally isotropic and the shear modulus, G, is related to the Young's modulus, E, by $G = \frac{E}{2(1+\nu)}$, where ν is the Poisson's ratio and $0 \leq \nu \leq 1$. Thus $\frac{E}{4} \leq G \leq \frac{E}{2}$. On the other hand, the shear modulus in composite materials is much less than the Young's modulus and so the transverse shear cannot be neglected [KWON and BANG, 1997]. Transverse shear also affects thick composite beams or laminated beams, with widely differing material properties, therefore, the classical Euler-Bernoulli theory is not appropriate for modelling the bending behaviour of composite sandwich beams. A more appropriate beam theory for modelling the flexural behaviour of composite sandwich beams is the Timoshenko beam theory [TESSLER et al., 2009, TIMOSHENKO, 1921]. The Timoshenko beam theory allows for transverse shear by relaxing the third assumption of the Euler-Bernoulli. Consequently, the Timoshenko beam theory is based on the following assumptions:

1. Transverse normals of the beam remain straight after deformation.

2. The length of the transverse normals remains unaltered after deformation.

1.3 Objectives of this study

The objectives of this study are set as follows

- Develop numerical algorithm for the bending of a linear and nonlinear composite sandwich beam.
- Implement the numerical algorithm in MATLAB using the finite element method.
- Validate the numerical results by comparison with the data provided by the CSIR Research Facilities in Port Elizabeth.
- Implement the cohesive zone modelling technique using the MSC Software Corporation's software packages MSC.Marc and MSC.Mentat [MSC.Software, 2007] by applying the cohesive zone interface modelling.
- Numerically simulate delamination of the composite sandwich panel.

1.4 Thesis Layout

Chapter 2 Uses the principle of virtual work to derive the equations and boundary conditions governing both linear and nonlinear Timoshenko beam theory.

Chapter 3 Derives the finite element model and numerical algorithm for the equations derived in Chapter 2.

Chapter 4 Reviews delamination theory with particular reference to the cohesive zone model finally developing the interface elements for the cohesive zone A mixed mode interface element formulation based on the bilinear traction-relative displacement relation is developed.

Chapter 5 We then carry out a delamination simulation case study of the composite sandwich beam in MSC.Marc and MSC.Mentat. We base the delamination simulation on the delamination theory we developed in Chapter 3. We then compare the results to experimental results..

Chapter 6 Will end the study, summarising the results and giving recommendations for further work.

Chapter 2
Theoretical Framework

This chapter reviews the Timoshenko beam theory for the linear and nonlinear models. We will use the principle of virtual work to derive the governing equations and boundary conditions. The derivation follows from the derivation of the first order shear deformation theory found in literature [REDDY, 2004]. The first order shear deformation theory is a 2D version of the Timoshenko beam theory and as such, reduction of the first order shear deformation theory to the Timoshenko beam theory follows naturally.

2.1 Principle of virtual work

We begin by introducing the principle of virtual work, which we will use in this chapter to determine the governing equations. Virtual work arises because of virtual displacements, which are assumed displacements of a body which do not violate the constraints or boundary conditions of the system. The principle of virtual work for a static body in equilibrium [BELYTSCHKO et al., 2000] is stated as follows

Definition 1 *The virtual work done by all actual forces in moving a continuous body through a virtual displacement is zero.:*

$$\delta U_{int} + \delta V_{ext} = 0 \tag{2.1}$$

where δU_{int} is the virtual strain energy and δV_{ext} is the virtual work done by applied forces.

Equivalently, the virtual work done by external forces to move a body through a virtual displacement is equal to the increase in virtual strain energy or the virtual internal power of the body. The principle of virtual work thus serves as an alternative form of the principle of energy but this time in a virtual sense.

2.2 Linear Timoshenko beam theory

In the first part of the analysis, we restrict our analysis to small strains and rotations to create a linear model.

2.2.1 Displacement and linear strains

Fig (2.2) gives a general representation of the Timoshenko Beam Theory. Under the assumptions of the Timoshenko beam theory and the restrictions as in the classical Euler-Bernoulli theory, the displacement field of the Timoshenko beam theory for pure bending is of the form

$$u\left(x,z\right)=z\Psi\left(x\right) \tag{2.2}$$

$$w\left(x,z\right)=W\left(x\right) \tag{2.3}$$

where W is the displacement component along the z coordinate direction of a point on the midline. In pure bending, there is no axial load resulting in $u_0 = 0$, see Fig (2.2). For the first part of our analysis, we are focusing on the linear analysis; therefore, we will use

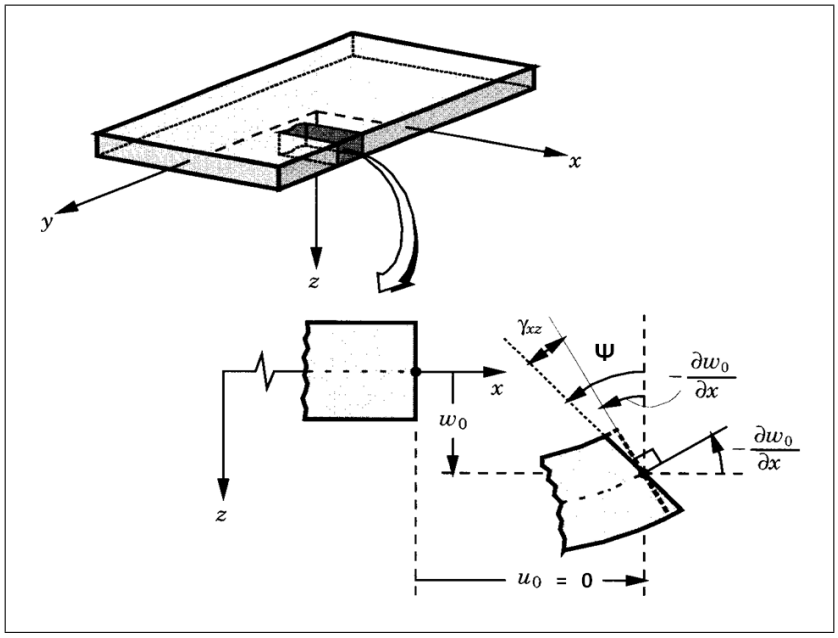

Fig. 2.2. Beam bending under Timoshenko beam theory, reproduced from Mechanics of Laminated Composite Plates and Shells, J.N. Reddy, 2004, page 133.

the displacement field given by equations (2.2) and (2.3) to obtain the linear stresses. We obtain the linear stresses by applying the infinitesimal strain tensor as defined by REDDY (2008)

$$\varepsilon_{ij} = \frac{1}{2}\left(\frac{\partial u_i}{\partial x_j} + \frac{\partial u_j}{\partial x_i}\right) \tag{2.4}$$

where $(x_1, x_2, x_3) \equiv (x, y, z)$ and $(u_1, u_2, u_3) \equiv (u, v, w)$. See Appendix B for a discussion on the infinitesimal strain tensor.

In this study, $\frac{\partial}{\partial y}(\cdot) \equiv 0$ in all cases since we are analysing the composite sandwich panel as a beam. Applying the infinitesimal strain tensor to the Timoshenko beam displacement field, we obtain the following strains

$$\varepsilon_{xx} = z\frac{d\Psi}{dx} = z\varepsilon_{xx}^{(1)} \tag{2.5}$$

$$\gamma_{xz} = 2\varepsilon_{xz} = \Psi + \frac{dW}{dx} = \gamma_{xz}^{(0)} \tag{2.6}$$

The superscripts in $\gamma_{xz}^{(0)}$ and $\varepsilon_{xx}^{(1)}$ present a convenient notation for the strains, the $^{(0)}$ superscript representing membrane or in-plane strains and the $^{(1)}$ superscript representing the flexural or bending strains, known as curvatures.

2.2.2 Governing Equations

To obtain the governing equations through the principle of virtual work, consider a beam of length L [REDDY, 2004].

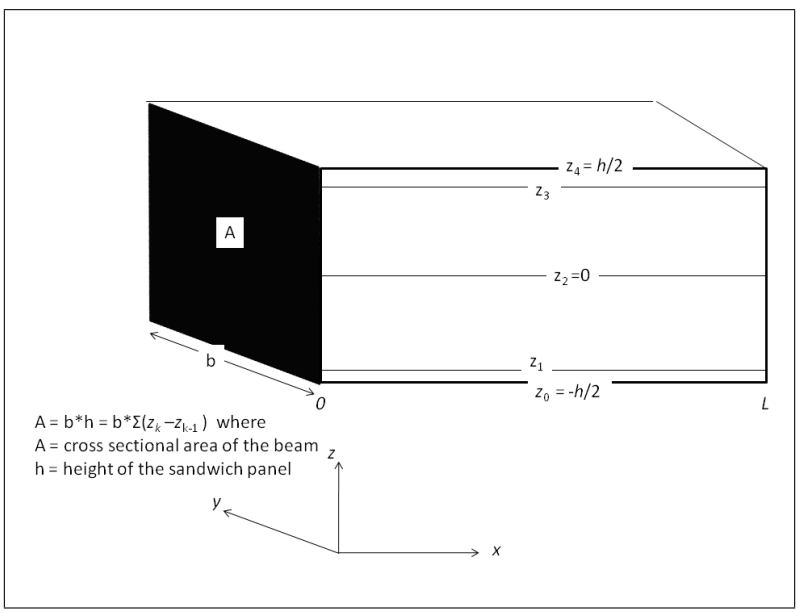

Fig. 2.3. Composite sandwich beam of length L

Let $f = f(x)$ be a transverse load acting on the beam element producing a virtual transverse displacement δW. The virtual work done by the actual load $f(x)$ is given by

$$\delta V_{ext} = -\int_0^L (f\delta W)\, dx \tag{2.7}$$

The applied force induces stresses in the beam, σ_{xx} and τ_{xz}, causing the beam to undergo virtual strains $\delta\varepsilon_{xx}$ and $\delta\gamma_{xz}$. The virtual strain energy caused by the actual stresses σ_{xx} and τ_{xz} is given by

$$\delta U_{int} = \int_0^L \int_A (\sigma_{xx}\delta\varepsilon_{xx} + \tau_{xz}\delta\gamma_{xz})\, dAdx \tag{2.8}$$

where $A = b\sum_{k=1}^{4}(z_k - z_{k-1})$, the cross sectional area of the beam, b is the width of the sandwich panel., and we are taking the summation from $k = 1$ to $k = 4$ because of the four layers created by diving the core into two layers at the midline.

Employing the fact that $\int_A (\cdot)\, dA = b\int_{-h/2}^{h/2}(\cdot)\, dz = b\sum_{k=1}^{4}\int_{z_{k-1}}^{z_k}(\cdot)\, dz$, equation (2.8) reduces to

$$\delta U_{int} = b\int_0^L \int_{-h/2}^{h/2} (\sigma_{xx}\delta\varepsilon_{xx} + \tau_{xz}\delta\gamma_{xz})\, dzdx \tag{2.9}$$

Integrating through the thickness of the composite sandwich beam on a layer-by-layer basis results in

$$\delta U_{int} = b\sum_{k=1}^{4}\int_0^L \int_{z_{k-1}}^{z_k} \left(\sigma_{xx} z\delta\varepsilon_{xx}^{(1)} + \tau_{xz}\delta\gamma_{xz}^{(0)}\right) dzdx \tag{2.10}$$

$$\delta U_{int} = \int_0^L \left(M_{xx}\delta\varepsilon_{xx}^{(1)} + Q_x\delta\gamma_{xz}^{(0)}\right) dx \tag{2.11}$$

where the shear and moment resultants through the thickness of the four layers of the composite sandwich beam are defined as

$$Q_x = bK\sum_{k=1}^{4}\int_{z_{k-1}}^{z_k} \tau_{xz} dz \tag{2.12}$$

$$M_{xx} = b\sum_{k=1}^{4}\int_{z_{k-1}}^{z_k}\sigma_{xx}zdz \tag{2.13}$$

where K, the shear correction coefficient, is introduced to correct the discrepancy between the constant stress state through the thickness given by the laminate constitutive relations and the true stress state through the thickness, which is parabolic [REDDY, 2004]. See the discussion on K in section 2.2.4.

Since $\varepsilon_{xx}^{(1)} = \frac{d\Psi}{dx}$ and employing the fact that $\delta\Psi$ and δW represent virtual displacements, the virtual internal energy reduces to

$$\delta U_{int} = \int_0^L \left\{ M_{xx}\left(\frac{d\left(\delta\Psi\right)}{dx}\right) + Q_x\left(\delta\Psi + \frac{d\left(\delta W\right)}{dx}\right)\right\} dx \tag{2.14}$$

Integrating by parts results in

$$\begin{aligned}\delta U_{int} &= \int_0^L \left\{ -\frac{dM_{xx}}{dx}\delta\Psi + Q_x\delta\Psi - \frac{dQ_x}{dx}\delta W\right\} dx + \\ &\quad [M_{xx}\delta\Psi]_0^L + [Q_x\delta W]_0^L \end{aligned} \tag{2.15}$$

Since we now have δU_{int} and δV_{ext}, we obtain the principle of virtual work for the linear Timoshenko beam theory as

$$\int_0^L \left(\frac{dQ_x}{dx} + f\right)\delta W dx + \int_0^L \left(\frac{dM_{xx}}{dx} - Q_x\right)\delta\Psi dx$$

$$= [M_{xx}\delta\Psi]_0^L + [Q_x\delta W]_0^L \tag{2.16}$$

The Fundamental Theorem of Variational Calculus If

$$\int_{x_0}^{x_1} \rho(x)\,\eta(x)\,dx + B(x_0)\,\eta(x_0) + B(x_1)\,\eta(x_1) = 0 \tag{2.17}$$

where $\rho(x)$ is a piecewise continuous function of x, $B(x_0)$ and $B(x_1)$ are yet undetermined coefficients of x, $\eta(x)$ is an arbitrary continuous function in $x_0 < x < x_1$, $\eta(x_0)$ and $\eta(x_1)$ are arbitrary, then $\rho(x) \equiv 0$ and $B(x_0) = 0$ and $B(x_1) = 0$ [HJELMSTAD, 2005, MURA and KOYA, 1992].

Since δW and $\delta\Psi$ are arbitrary in $(0, L)$, employing the fundamental theorem of variational calculus in equation (2.16), we obtain the equilibrium or Euler-Lagrange equations by setting the coefficients of δW and $\delta\Psi$ to zero separately:

$$\frac{dQ_x}{dx} + f = 0 \tag{2.18}$$

$$\frac{dM_{xx}}{dx} - Q_x = 0 \tag{2.19}$$

If we make δW and $\delta\Psi$ arbitrary at the boundary points, we obtain the natural boundary conditions by setting the coefficients of δW and $\delta\Psi$ to zero separately resulting in the following natural boundary conditions at $x = 0$ or $x = L$

$$Q_x = 0 \qquad \text{or} \qquad M_{xx} = 0 \tag{2.20}$$

2.2.3 Laminate Constitutive Relations

To obtain the sandwich beam constitutive equations from the Euler-Lagrange equations, we introduce the laminate constitutive relations from Hooke's Law, so that for the kth layer,

we have

$$\begin{Bmatrix} \sigma_{xx} \\ \tau_{xz} \end{Bmatrix}^k = \begin{bmatrix} E_{xx}^k & 0 \\ 0 & G_{xz}^k \end{bmatrix} \begin{Bmatrix} \varepsilon_{xx}^{(1)} \\ \gamma_{xz}^{(0)} \end{Bmatrix} \tag{2.21}$$

Thus equations (2.12) and equation (2.13) become

$$Q_x = bK \sum_{k=1}^{4} \int_{z_{k-1}}^{z_k} G_{xz}^k \gamma_{xz}^{(0)} = (GA)_{equi} K \gamma_{xz}^{(0)} \tag{2.22}$$

$$M_{xx} = b \sum_{k=1}^{4} \int_{z_{k-1}}^{z_k} E_{xx}^k \left[z \varepsilon_{xx}^{(1)} \right] z dz = (EI)_{equi} \varepsilon_{xx}^{(1)} = D_{xx} \varepsilon_{xx}^{(1)} \tag{2.23}$$

where:

$$(EI)_{equi} = \frac{b}{3} \sum_{k=1}^{4} E_{xx}^{(k)} \left(z_k^3 - z_{k-1}^3 \right) \tag{2.24}$$

where $(EI)_{equi}$ is the equivalent flexural rigidity or the bending stiffness of the sandwich panel and $E_{xx}^{(k)}$ is the Young's modulus of the kth layer; where $(GA)_{equi} = \sum_{k=1}^{4} bG_{xz}^{(k)} (z_k - z_{k-1})$ is the equivalent shear modulus of the beam and $G_{xz}^{(k)} =$ the shear modulus of the kth layer.

For clarity, we will omit the subscripts from $(GA)_{equi}$ and $(EI)_{equi}$ and simply define

$$GA \equiv (GA)_{equi} \quad \text{and} \quad EI \equiv (EI)_{equi} \tag{2.25}$$

Note the D_{xx} is just an alternative form for EI and we use it out of convenience in the calculation of K.

Inserting (2.21) into (2.18) and (2.19), we obtain the following equilibrium equations:

$$\frac{d}{dx} \left(GAK \left(\frac{dW}{dx} + \Psi \right) \right) + f = 0 \tag{2.26}$$

$$\frac{d}{dx} \left(EI \frac{d\Psi}{dx} \right) - GAK \left(\frac{dW}{dx} + \Psi \right) = 0 \tag{2.27}$$

and the natural boundary conditions at $x = 0$ or $x = L$, namely

$$GAK\left(\frac{dW}{dx} + \Psi\right) = 0 \qquad \text{or} \qquad EI\frac{d\Psi}{dx} = 0 \tag{2.28}$$

2.2.4 Determination of the shear correction factor

Six different methods for calculating the shear correction factor, K, are discussed in the literature [BIRMAN and BERT, 2002]. Three of those methods give a value of unity for the shear correction factor while for the other three methods, the value varies as the geometry and/or stiffness varies. The methods in which the value varied with stiffness are the discrete-mass system method, the shear energies comparison method and average strain comparison method. Comparing the values obtained by the three different methods, it was found that in the case of the discrete-mass system method, the method gave widely differing values with the correction factor value increasing unacceptably as core-to-facesheet thickness ratio increased, approaching unity. The value obtained using the average shear strain method decreased very marginally as the core-to-facesheet thickness ratio increased approaching unity but dropped sharply as the core shear modulus decreased. Finally, the shear strain energy method gave very low values for core-to-facesheet thickness ratios increasing towards unity.

With these results, we can conclude that we can use the factor methods depending on stiffness and geometry and geometry in those cases where the thickness of the facesheet is negligible compared to the thickness of the facesheet. BIRMAN and BERT

suggested a universal value of $K = 1$ for all composite sandwich structures though SKAWINSKI et al. (2004) later used the shear strain energy comparison method to get the shear correction factor and obtained numerical results which compared favourably with experimental results for the bending of a five-layer thermoplastic composite sandwich plate. We detail the shear strain energy method below as derived by SKAWINSKI et al. (2004). Similar results can be obtained by following alternative approaches in literature [MADABHUSI-RAMAN and DAVALOS, 1996].

Recall from equation (2.22) that the shear stress resultant from the constitutive relations is given by

$$Q_x = GAK\gamma_{xz}^{(0)} \tag{2.29}$$

The general equilibrium equations for an arbitrary body with no body forces or surface tractions is obtained from the conservation of linear momentum as [BELYTSCHKO et al., 2000]:

$$\nabla \cdot \boldsymbol{\sigma} = 0 \tag{2.30}$$

where σ represents the generalised stresses on the body.

$$\boldsymbol{\sigma} = \begin{bmatrix} \sigma_{xx} & \tau_{xy} & \tau_{xz} \\ \tau_{xy} & \sigma_{yy} & \tau_{yz} \\ \tau_{xz} & \tau_{yz} & \sigma_{zz} \end{bmatrix} \tag{2.31}$$

From these general equilibrium equations, the equilibrium equation in the x-direction for the kth layer is given as

$$\frac{\partial \sigma_{xx}^k}{\partial x} + \frac{\partial \tau_{xz}^k}{\partial z} = 0 \tag{2.32}$$

The moment equilibrium about the y-direction gives

$$\frac{\partial M_{xx}}{\partial x} = Q_x \tag{2.33}$$

Recall from equation (2.23) that

$$M_{xx} = D_{xx}\varepsilon_{xx}^{(1)} = D_{xx}\kappa_x \tag{2.34}$$

where $\kappa_x = \varepsilon_{xx}^{(1)}$, the curvature of x.

The in-plane stresses for the composite sandwich beam are given by

$$\sigma_{xx}^k = zE_{xx}^k\kappa_x \tag{2.35}$$

Combining (2.35) and (2.34), we can express the normal stress σ_{xx}^k as a function of the moment M_{xx} [SKAWINSKI et al., 2004]:

$$\sigma_{xx}^k = zE_{xx}^k d_{xx}M_{xx} \tag{2.36}$$

where $d_{xx} = (D_{xx})^{-1}$. Equation (2.36) can also be expressed as:

$$\sigma_{xx}^k = zB_{x2}^k M_{xx} \tag{2.37}$$

where $B_{x2}^k = E_{xx}^k d_{xx}$.

Substituting for (2.37) in the equilibrium equation (2.32) gives

$$\frac{\partial\tau_{xz}^k}{\partial z} = -\left(zB_{x2}^k\right)Q_x \tag{2.38}$$

Integrating equation (2.38) through the thickness yields

$$\tau_{xz}^k = \int_{z_{k-1}}^{z} -\left(\xi B_{x2}^k\right)Q_x d\xi = -\frac{1}{2}\left(z^2 - z_{k-1}^2\right)B_{x2}^k Q_x + H^k(x) \tag{2.39}$$

We now apply the following boundary conditions to determine $H^k(x)$:

$\tau_{xz}^1 = 0$ at $z = z_0 = -\frac{h}{2}$;

$\tau_{xz}^k = \tau_{xz}^{k+1}$ at $z = z_k$;

$\tau_{xz}^N = 0$ at $z = z_{N+1} = \frac{h}{2}$.

From the interlayer boundary condition, equating τ_{xz}^{k} and τ_{xz}^{k+1} at $z = z_k$, we get that

$$-\frac{1}{2}\left(z_k^2 - z_{k-1}^2\right) B_{x2}^{k} Q_x + H^k = H^{k+1} \tag{2.40}$$

and on re-arranging, obtain

$$H^{k+1} - H^k = -\frac{1}{2}\left(z_k^2 - z_{k-1}^2\right) B_{x2}^{k} Q_x \tag{2.41}$$

Setting $k = 1$ and substituting for $z = z_0$ in equation (2.39) yields

$$H^1 = 0 \tag{2.42}$$

Likewise from the third boundary condition, setting $k = N+1$ substituting for $z = z_N = \frac{h}{2}$ in equation (2.39) gives

$$H^{N+1} = 0 \tag{2.43}$$

From equation (2.41) , substituting for $k = 1$ in the expression gives

$$H^2 = -\frac{1}{2}\left(z_1^2 - z_0^2\right) B_{x2}^{1} Q_x + H^1 = -\frac{1}{2}\left(z_1^2 - z_0^2\right) B_{x2}^{1} Q_x \tag{2.44}$$

and

$$H^3 = -\frac{1}{2}\left(z_2^2 - z_1^2\right) B_{x2}^{2} Q_x + H^2 \tag{2.45}$$

$$= -\frac{1}{2}\left(z_2^2 - z_1^2\right) B_{x2}^{2} Q_x - \frac{1}{2}\left(z_1^2 - z_0^2\right) B_{x2}^{1} Q_x \tag{2.46}$$

Therefore, H^{k+1} can be written recursively as

$$H^{k+1} = \sum_{j=1}^{k}\left(-\frac{1}{2}\left(z_j^2 - z_{j-1}^2\right) B_{x2}^{j} Q_x\right) \tag{2.47}$$

or

$$H^{k} = \sum_{j=1}^{k-1}\left(-\frac{1}{2}\left(z_j^2 - z_{j-1}^2\right) B_{x2}^{j} Q_x\right) \tag{2.48}$$

Define

$$B_{x0}^{k} = \sum_{j=1}^{k-1} \left(-\frac{1}{2} \left(z_j^2 - z_{j-1}^2 \right) B_{x2}^{j} Q_x \right) \tag{2.49}$$

then we can finally write the composite sandwich beam shear stress for the kth layer as

$$\tau_{xz}^{k} = -\left(\frac{1}{2} \left(z^2 - z_{k-1}^2 \right) B_{x2}^{k} + B_{x0}^{k} \right) Q_x \tag{2.50}$$

Further, define $g_{55}^{k} = -\left(\frac{1}{2} \left(z^2 - z_{k-1}^2 \right) B_{x2}^{k} + B_{x0}^{k} \right)$. Then

$$\tau_{xz}^{k} = g_{55}^{k} Q_x \tag{2.51}$$

The expression of shear strain energy for the composite sandwich beam is given by

$$U_{sc} = \frac{1}{2} \sum_{k=1}^{N} \int_{z_{k-1}}^{z_k} \left(\tau_{xz}^{k} \gamma_{xz}^{k} \right) dz \tag{2.52}$$

and since

$$\tau_{xz}^{k} = G_{xz}^{k} \gamma_{xz} \tag{2.53}$$

we obtain

$$U_{sc} = \frac{1}{2} \sum_{k=1}^{N} \int_{z_{k-1}}^{z_k} \frac{1}{G_{xz}^{k}} \left(\tau_{xz} \right)^2 dz \tag{2.54}$$

Substituting τ_{xz}, from equation (2.51) in equation (2.54) we get the following expression for transverse shear strain energy

$$U_{sc} = \frac{1}{2} \sum_{k=1}^{N} \int_{z_{k-1}}^{z_k} \frac{1}{G_{xz}^{k}} \left(g_{55}^{k} \right)^2 dz \left(Q_x \right)^2 \tag{2.55}$$

Similarly, the shear strain energy computed from the constitutive relation of equation (2.29) which assumes constant transverse shear strain, is

$$U_{sc} = \frac{1}{2KGA} \left(Q_x \right)^2 \tag{2.56}$$

Equating equations (2.55) and (2.56) , we get the expression for the shear correction factor given by

$$K = \frac{1}{GA} \cdot \frac{1}{\sum_{k=1}^{N} \int_{z_{k-1}}^{z_k} \frac{1}{G_{xz}^k} \left(g_{55}^k\right)^2 dz} \tag{2.57}$$

2.3 Nonlinear Timoshenko Beam Theory

The linear model is valid for small strains and small rotations. However, we want to study the geometrical nonlinear behaviour of composite sandwich beams, where the nonlinearity will be included in the form of von Karmann nonlinear strains by replacing the infinitesimal strain tensor with the Green strain tensor. The Green strain tensor also assumes small strains but mild rotations.

2.3.1 Timoshenko beam theory displacements and nonlinear strains

The displacement field remains unchanged and is repeated here for completion

$$u\left(x, z\right) = z\Psi\left(x\right) \tag{2.58}$$

$$w\left(x, z\right) = W\left(x\right) \tag{2.59}$$

For nonlinear finite element analysis, we relax the restriction of small displacements and strains and employ the Green strain tensor to get the strains, defined as [REDDY, 2008, LAI et al., 1993]

$$\varepsilon_{ij} = \frac{1}{2}\left(\frac{\partial u_i}{\partial x_j} + \frac{\partial u_j}{\partial x_i} + \frac{\partial u_m}{\partial x_i}\frac{\partial u_m}{\partial x_j}\right) \tag{2.60}$$

Note that the summation convention is assumed. See Appendix B for a discussion on the Green strain tensor.

Applying the Green strain tensor to the displacement field given by equations (2.58) and (2.59) gives the following strains:

$$\varepsilon_{xx} = \frac{1}{2}\left(\frac{dW}{dx}\right)^2 + z\frac{d\Psi}{dx} \tag{2.61}$$

$$\gamma_{xz} = \gamma_{xz}^{(0)} = \Psi + \frac{dW}{dx} \tag{2.62}$$

2.3.2 Governing equations

For the principle of virtual work terms, δV_{ext} remains unchanged as

$$\delta V_{ext} = -\int_0^L (f\delta W)\, dx \tag{2.63}$$

whilst δU_{int} becomes

$$\delta U_{int} = \sum_{k=1}^{4} \int_0^L \int_{z_{k-1}}^{z_k} b\left(\sigma_{xx}\delta\varepsilon_{xx} + \tau_{xz}\delta\gamma_{xz}\right) dz dx \tag{2.64}$$

reducing to

$$\delta U_{int} = \int_0^L \left(N_{xx}\delta\varepsilon_{xx}^{(0)} + M_{xx}\delta\varepsilon_{xx}^{(1)} + Q_x\delta\gamma_{xz}^{(0)}\right) dx \tag{2.65}$$

where

$$\varepsilon_{xx}^{(0)} = \frac{1}{2}\left(\frac{dW}{dx}\right)^2 \tag{2.66}$$

$$N_{xx} = \sum_{k=1}^{4} \int_{z_{k-1}}^{z_k} \left(b\sigma_{xx}^k\right) dz \tag{2.67}$$

and $\varepsilon_{xx}^{(1)}$, $\gamma_{xz}^{(0)}$, M_{xx} and Q_x defined as before.

Since all the other terms in δU_{int} are the same in the nonlinear analysis, it is sufficient to consider the integral of the first term in δU_{int} and use the previous results for the other terms. From equation (2.66) , taking variations gives

$$\delta\varepsilon_{xx}^{(0)} = \frac{dW}{dx}\frac{d\left(\delta W\right)}{dx} \tag{2.68}$$

Now,

$$\int_0^L \left(N_{xx}\delta\varepsilon_{xx}^{(0)}\right) dx = \int_0^L \left(N_{xx}\frac{dW}{dx}\frac{d\left(\delta W\right)}{dx}\right) dx \tag{2.69}$$

Therefore

$$\delta U_{int} = \int_0^L \left\{N_{xx}\frac{dW}{dx}\frac{d\left(\delta W\right)}{dx} + M_{xx}\frac{d\left(\delta\Psi\right)}{dx} + Q_x\left(\delta\Psi + \frac{d\left(\delta\Psi\right)}{dx}\right)\right\} dx \tag{2.70}$$

Integrating by parts the terms in δU_{int} to get rid of the derivatives of the variations results in

$$\begin{aligned}\delta U_{int} &= \int_0^L \left\{-\frac{d}{dx}\left(N_{xx}\frac{dW}{dx}\right)\delta W - \frac{dM_{xx}}{dx}\delta\Psi + Q_x\delta\Psi - \frac{dQ_x}{dx}\delta W\right\} dx \\ &\quad + \left[\left(Q_x + N_{xx}\frac{dW}{dx}\right)\delta W\right]_0^L + \left[M_{xx}\delta\Psi\right]_0^L \end{aligned} \tag{2.71}$$

finally giving us the following expression from the principle of virtual work

$$\begin{aligned}&\int_0^L \left(\frac{d}{dx}\left(N_{xx}\frac{dW}{dx}\right) + \frac{dQ_x}{dx} + f\right)\delta W dx + \int_0^L \left(\frac{dM_{xx}}{dx} - Q_x\right)\delta\Psi dx \\ &= \left[\delta W\left(Q_x + N_{xx}\frac{dW}{dx}\right)\right]_0^L + \left[M_{xx}\delta\Psi\right]_0^L \end{aligned} \tag{2.72}$$

Employing the fundamental theorem of variational calculus, since δW and $\delta\Psi$ are arbitrary on $(0, L)$, we obtain the Euler-Lagrange equations by setting the coefficients of δW and $\delta\Psi$ to zero separately:

$$\frac{d}{dx}\left(N_{xx}\frac{dW}{dx} + Q_x\right) + f = 0 \tag{2.73}$$

$$\frac{dM_{xx}}{dx} - Q_x = 0 \tag{2.74}$$

and making δW and $\delta\Psi$ arbitrary at the boundary points, we obtain the following natural boundary conditions at points $x = 0$ or $x = L$

$$Q_x + N_{xx}\frac{dW}{dx} = 0 \qquad \text{or} \qquad M_{xx} = 0 \tag{2.75}$$

Clearly, these nonlinear Euler-Lagrange equations are the same as the linear equations, with the exception of the nonlinear term, $\frac{d}{dx}\left(N_{xx}\frac{dW}{dx}\right)$.

2.3.3 Laminate Constitutive Relations

We again use the following laminate constitutive relations to obtain the Timoshenko beam equations:

$$\begin{Bmatrix} \sigma_{xx} \\ \tau_{xz} \end{Bmatrix}^k = \begin{bmatrix} E_{xx}^k & 0 \\ 0 & G_{xz}^k \end{bmatrix} \begin{Bmatrix} \varepsilon_{xx}^{(1)} \\ \gamma_{xz}^{(0)} \end{Bmatrix} \tag{2.76}$$

Recall that

$$M_{xx} = EI\varepsilon_{xx}^{(1)} \tag{2.77}$$

and

$$Q_x = GAK\gamma_{xz}^{(0)} \tag{2.78}$$

we define the following stress resultant, namely

$$N_{xx} = \sum_{k=1}^{4}\int_{z_{k-1}}^{z_k}(b\sigma_{xx})\,dz = \sum_{k=1}^{4}\int_{z_{k-1}}^{z_k} bE_{xx}^k\left(\varepsilon_{xx}^{(0)}\right)dz = (EA)_{equi}\,\varepsilon_{xx}^{(0)} \tag{2.79}$$

where

$$(EA)_{equi} = b\sum_{k=1}^{4} E_{xx}^k\left(z_k - z_{k-1}\right) \tag{2.80}$$

Dropping the subscript for brevity, we finally have

$$N_{xx} = EA\varepsilon_{xx}^{(0)} \tag{2.81}$$

Substituting for N_{xx} in equation (2.73) and using the expressions for M_{xx} and Q_x from the linear analysis, we obtain the following equilibrium equations:

$$\frac{d}{dx}\left(\frac{EA}{2}\left(\frac{dW}{dx}\right)^2\right) + \frac{d}{dx}\left(GAK\left(\frac{dW}{dx} + \Psi\right)\right) + f = 0 \tag{2.82}$$

and

$$\frac{d}{dx}\left(EI\frac{d\Psi}{dx}\right) - GAK\left(\frac{dW}{dx} + \psi\right) = 0 \tag{2.83}$$

with the natural boundary terms at $x = 0$ or $x = L$, namely

$$GAK\left(\frac{dW}{dx} + \Psi\right) + \frac{EA}{2}\left(\frac{dW}{dx}\right)^2 = 0 \qquad \text{or} \qquad EI\frac{d\Psi}{dx} = 0 \tag{2.84}$$

Chapter 3
Finite Element Analysis

As an effective and cost saving alternative to conducting numerous experiments, numerical methods can greatly reduce material design time by simulating a variety of materials and loading conditions. The most commonly used methods are the finite difference, finite volume and finite element methods. While the finite difference is well described and simple to implement, it is the finite element method which has become the industry method of choice.

The finite element method was originally developed to study the stresses in coupled air-frame structures [CLOUGH, 1960] and will be used in this study. The method approximates the problem domain by a finite number of non-intersecting but interconnected sub-domains called elements [RAO, 2005]. Each neighbouring element shares a boundary with either other elements or with the domain boundary. Whether this common boundary can be represented by a point, a line or a surface depends on the dimension of the original problem [REDDY, 1993]. The geometry of each subdomain or element is identified by nodal points or nodes and the nodes are used to generate simple algebraic polynomials which are used to approximate the solution. The global solution is then obtained by pairing together the local element approximations, enforcing continuity of the global solution or field variable. Thus the global solution can be seen to be obtained from the local nodal values [ZIENKIEWICZ and TAYLOR, 2000]. Unlike the finite difference method, the finite element method is locally suitable for solving complex problem domains. Employing

these approximations reduces the governing equations to a system of either linear or non-linear algebraic equations from which the nodal values of the solution (field variables) can be obtained.

Employing the finite element method to approximate the solution to a continuum problem is carried out using the steps below [RAO, 2005]

1. Discretise the problem domain into a collection on non-overlapping elements.
2. Obtain the weak formulation of governing equations over a typical finite element.
3. Select appropriate interpolation functions. This will heavily depend on the number of nodes used to define the element.
4. Derive the element equations, that is, the element stiffness matrix and element load vector.
5. Assemble the element equations and obtain the governing equations.
6. Implement the boundary conditions and solve for the unknown nodal displacements.
7. Compute the secondary quantities from the nodal solution values and obtain the element stresses and strains.

We shall now apply the step-by-step procedure to solve the problem of Timoshenko beam subjected to a four-point load. The approach presented by REDDY (1993) will be employed.

3.1 Linear finite element analysis

Step 1 Mesh the beam simply dividing the beam length into N equal elements with nodes $x_1, x_2, ..., x_{N+1}$.

Step 2 Recall from equation (2.26) and equation (2.27) that the governing equations for the Timoshenko beam theory are given by

$$\frac{d}{dx}\left(GAK\left(\frac{dW}{dx}+\Psi\right)\right)+f = 0 \tag{3.85}$$

$$\frac{d}{dx}\left(EI\frac{d\Psi}{dx}\right)-GAK\left(\frac{dW}{dx}+\Psi\right) = 0 \tag{3.86}$$

To obtain the associated weak formulation, we premultiply each equation with a suitably selected weight or test function and integrate over an arbitrary element $\Omega^e = (x_e, x_{e+1})$. The test functions must be smooth enough to satisfy the same continuity requirements for W and Ψ.

Multiplying the governing equations by the test functions v_1 and v_2 and integrating over the element, we obtain

$$\int_{x_e}^{x_{e+1}} v_1\left\{\frac{d}{dx}\left(GAK\left(\frac{dW}{dx}+\Psi\right)\right)+f\right\}dx = 0 \tag{3.87}$$

$$\int_{x_e}^{x_{e+1}} v_2\left\{\frac{d}{dx}\left(EI\frac{d\Psi}{dx}\right)-GAK\left(\frac{dW}{dx}+\Psi\right)\right\}dx = 0 \tag{3.88}$$

Now distribute the derivative evenly between field variables and the test functions. This is achieved using integration by parts, resulting in

$$\int_{x_e}^{x_{e+1}} \left\{ \frac{d\left(v_1\right)}{dx} \left(GAK \left(\frac{dW}{dx} + \Psi \right) \right) - f v_1 \right\} dx = \left[\left(GAK \left(\frac{dW}{dx} + \Psi \right) \right) v_1 \right]_{x_e}^{x_{e+1}} \tag{3.89}$$

$$\int_{x_e}^{x_{e+1}} \left\{ \frac{d\left(v_2\right)}{dx} \left(EI \frac{d\Psi}{dx} \right) + GAK \left(\frac{dW}{dx} + \Psi \right) v_2 \right\} dx = \left[EI \frac{d\Psi}{dx} v_2 \right]_{x_e}^{x_{e+1}} \tag{3.90}$$

Step 3 From equations (2.22) and (2.23), we have

$$GAK \left(\frac{dW}{dx} + \Psi \right) \equiv Q_x \tag{3.91}$$

and

$$EI \frac{d\Psi}{dx} \equiv M_{xx} \tag{3.92}$$

where Q_x is the shear resultant and M_{xx} is the moment resultant. Out of convenience, we thus introduce the following notation [REDDY, 1993]

$$-GAK \left(\frac{dW}{dx} + \Psi \right) |_{x_e} = Q_1^e \qquad GAK \left(\frac{dW}{dx} + \Psi \right) |_{x_{e+1}} = Q_3^e \tag{3.93}$$

and

$$-EI \frac{d\Psi}{dx} |_{x_e} = Q_2^e \qquad EI \frac{d\Psi}{dx} |_{x_{e+1}} = Q_4^e \tag{3.94}$$

Since both W and Ψ are the primary variables and not their derivatives, Lagrange interpolation would appear appropriate. This follows from the fact that we only require $\frac{dW}{dx}$ and $\frac{d\Psi}{dx}$ to be nonzero. Further, since they don't have same units, they can be interpolated with different degrees of interpolation. For simplicity, we shall employ linear interpolation

so that W and Ψ have the form

$$W = \sum_{j=1}^{2} \psi_j^{(1)} w_j = \psi_1^{(1)} w_1 + \psi_2^{(1)} w_2 \tag{3.95}$$

$$\Psi = \sum_{j=1}^{2} \psi_j^{(2)} s_j = \psi_1^{(2)} s_1 + \psi_2^{(2)} s_2 \tag{3.96}$$

where

$$\psi_1^{(1)} = \psi_1^{(2)} = \frac{x_{e+1} - x}{x_{e+1} - x_e} = \frac{x_{e+1} - x}{l} \tag{3.97}$$

$$\psi_2^{(1)} = \psi_2^{(2)} = \frac{x - x_e}{x_{e+1} - x_e} = \frac{x - x_e}{l} \tag{3.98}$$

and

$$l = x_{e+1} - x_e \tag{3.99}$$

The $\psi^{(1)}$ and $\psi^{(2)}$ are the linear Lagrange interpolating functions and l is the element length.

Equal-order linear interpolation presents problems for thin or slender beams. For such beams, the linear element does not accurately model the bending behaviour. Recall from the Timoshenko beam theory that the transverse shear strain is given by

$$\gamma_{xz}^{(0)} = \Psi + \frac{dW}{dx} \tag{3.100}$$

For thin beams, [REDDY, 1993] the shearing strain, $\gamma_{xz}^{(0)}$, is negligible. Therefore, from equation (3.100), we have

$$\Psi = -\frac{dW}{dx} \tag{3.101}$$

From equations (3.95) and (3.96) , the above equation yields

$$\frac{x_{e+1} - x}{l} s_1 + \frac{x - x_e}{l} s_2 = -\frac{w_2 - w_1}{l} \tag{3.102}$$

or equivalently

$$x_{e+1} s_1 - x_e s_2 + (s_2 - s_1)\, x = -(w_2 - w_1) \tag{3.103}$$

Equating coefficients gives

$$s_2 - s_1 = 0 \tag{3.104}$$

$$x_{e+1}s_1 - x_e s_2 = -(w_2 - w_1) \tag{3.105}$$

resulting in

$$s_1 = s_2 = -\frac{w_2 - w_1}{l} \tag{3.106}$$

However, from equation (3.96) , we have that

$$\Psi = \frac{x_{e+1} - x}{l} s_1 + \frac{x - x_e}{l} s_2 = s_1 = s_2 = \text{constant} \tag{3.107}$$

The bending energy of the element is given by

$$\int_{x_e}^{x_{e+1}} \frac{EI}{2} \left(\frac{d\Psi}{dx} \right)^2 dx \tag{3.108}$$

and since Ψ is constant, it would imply that the bending energy is zero. Having a negligible bending energy compared to shear energy for a thin or slender beam is not physically correct, resulting in a numerical problem known as shear locking. As equal-order interpolation will be employed in this study $\left(\psi_i^{(1)} = \psi_i^{(2)}, \ \ i = 1, 2 \right)$, the problem of shear locking will be treated by selective-reduced integration [BELYTSCHKO et al., 2000, REDDY, 1993]. In selective-reduced integration, we under-integrate the shear terms whilst fully integrating the remainder of the matrix.

Integration of the stiffness matrix terms in commercial finite element analysis software is carried out using numerical integration due to the complexity of the integral expressions. See discussion on numerical integration.

Step 4 The element equations are obtained by substituting $W = \sum_{j=1}^{2} \psi_j^{(1)} w_j$ and $\Psi = \sum_{j=1}^{2} \psi_j^{(2)} s_j$ into equations (3.89) and (3.90) respectively, resulting in

$$\sum_{j=1}^{2} \left\{ \int_{x_e}^{x_{e+1}} \left(GAK \frac{d\psi_i^{(1)}}{dx} \frac{d\psi_j^{(1)}}{dx} \right) dx \right\} w_j \tag{3.109}$$

$$+ \sum_{j=1}^{2} \left\{ \int_{x_e}^{x_{e+1}} \left(GAK \frac{d\psi_i^{(1)}}{dx} \psi_j^{(2)} \right) dx \right\} s_j = \int_{x_e}^{x_{e+1}} f \psi_i^{(1)} dx + Q_{2i-1} \tag{3.110}$$

and

$$\sum_{j=1}^{2} \left\{ \int_{x_e}^{x_{e+1}} \left(GAK \psi_i^{(2)} \frac{d\psi_j^{(1)}}{dx} \right) dx \right\} w_j$$

$$+ \sum_{j=1}^{2} \left\{ \int_{x_e}^{x_{e+1}} \left(EI \frac{d\psi_i^{(2)}}{dx} \frac{d\psi_j^{(2)}}{dx} + GAK \psi_i^{(2)} \psi_j^{(2)} \right) dx \right\} s_j = Q_{2i} \tag{3.111}$$

after employing equations (3.93) and (3.94) in the boundary terms.

We can re-write the above equations in the following form:

$$\sum_{j=1}^{2} K_{ij}^{11} w_j + \sum_{j=1}^{2} K_{ij}^{12} s_j = F_i^1 \qquad i, j = 1, 2 \tag{3.112}$$

$$\sum_{j=1}^{2} K_{ij}^{21} w_j + \sum_{j=1}^{2} K_{ij}^{22} s_j = F_i^2 \qquad i, j = 1, 2 \tag{3.113}$$

where

$$K_{ij}^{11} = \int_{x_e}^{x_{e+1}} GAK \frac{d\psi_i^{(1)}}{dx} \frac{d\psi_j^{(1)}}{dx} dx \tag{3.114}$$

$$K_{ij}^{12} = \int_{x_i}^{x_{e+1}} GAK \frac{d\psi_i^{(1)}}{dx} \psi_j^{(2)} dx = K_{ji}^{21} \tag{3.115}$$

$$K_{ij}^{22} = \int_{x_e}^{x_{e+1}} \left(EI \frac{d\psi_i^{(2)}}{dx} \frac{d\psi_j^{(2)}}{dx} + GAK \psi_i^{(2)} \psi_j^{(2)} \right) dx \tag{3.116}$$

$$F_i^1 = \int_{x_e}^{x_{e+1}} f \psi_i^{(1)} dx + Q_{2i-1} \tag{3.117}$$

$$F_i^2 = Q_{2i} \tag{3.118}$$

We can write equations (3.112) and (3.113) in matrix form as:

$$\begin{bmatrix} [K^{11}] & [K^{12}] \\ [K^{21}] & [K^{22}] \end{bmatrix} \begin{Bmatrix} \{w\} \\ \{s\} \end{Bmatrix} = \begin{Bmatrix} \{F^1\} \\ \{F^2\} \end{Bmatrix} \tag{3.119}$$

3.1.1 Numerical Quadrature

The most widely used numerical integration procedure in finite elements is the Gauss quadrature [GOCKENBACH, 2006], and it is the one we will use in this study. The one dimensional Gauss quadrature formulas are

$$\int_{-1}^{1} f(\xi)\, d\xi = \sum_{i=1}^{n} w_i f(\xi_i) \tag{3.120}$$

where $\xi_1,\ \xi_2, ..., \xi_n\ \epsilon\ [-1, 1]$ are the quadrature nodes and $w_1,\ w_2, ..., w_n$ are the corresponding Gaussian weights. This n-point quadrature rule integrates $f(\xi)$ exactly if it is a polynomial of degree $m \leq 2n - 1$. The quadrature nodes and corresponding weights are available are available in Appendix A.

Consider the integral $\int_{x_e}^{x_{e+1}} g(x)dx$, then introducing the following linear change of variables:

$$x = x_e + \frac{l}{2}(\xi + 1) \tag{3.121}$$

where $l = x_{e+1} - x_e$, transforms the general integral $\int_{x_e}^{x_{e+1}} g(x)dx$ into the form $\int_{-1}^{1} f(\xi)\, d\xi$ such that

$$\int_{x_e}^{x_{e+1}} g(x)dx = \frac{l}{2}\int_{-1}^{1} f(\xi)\, d\xi \tag{3.122}$$

to which the Gaussian n-point rule (3.120) can be applied. We evaluate the matrix elements of the element stiffness matrix and the vector elements of the element nodal forces by

substituting for $g(x)$ by the appropriate integral expressions in (3.119) and then applying the Gaussian numerical procedure.

Using Gaussian quadrature, we can evaluate the element coefficient matrices K^{11}, K^{12} and the first part of K^{12} exactly, while for the second part of K^{22}, we use reduced integration.

Evaluating the stiffness matrix over master element, $\xi \epsilon [-1, 1]$, yields the following

$$\left[K^{11}\right] = \frac{GAK}{l}\begin{bmatrix} 1 & -1 \\ -1 & 1 \end{bmatrix}, \qquad \left[K^{12}\right] = \frac{GAK}{2}\begin{bmatrix} -1 & -1 \\ 1 & 1 \end{bmatrix} \tag{3.123}$$

$$\left[K^{22}\right] = \frac{EI}{l}\begin{bmatrix} 1 & -1 \\ -1 & 1 \end{bmatrix} + \frac{GAK}{4}\begin{bmatrix} 1 & 1 \\ 1 & 1 \end{bmatrix} \tag{3.124}$$

Therefore, the element equations become

$$\begin{bmatrix} \frac{GAK}{l} & -\frac{1}{2}GAK & -\frac{GAK}{l} & -\frac{1}{2}GAK \\ -\frac{1}{2}GAK & \frac{1}{4}GAK + \frac{EI}{l} & \frac{1}{2}GAK & \frac{1}{4}GAKl - \frac{EI}{l} \\ -\frac{GAK}{l} & \frac{1}{2}GAK & \frac{GAK}{l} & \frac{1}{2}GAK \\ -\frac{1}{2}GAK & \frac{1}{4}GAKl - \frac{EI}{l} & \frac{1}{2}GAK & \frac{1}{4}GAKh + \frac{EI}{l} \end{bmatrix} \begin{Bmatrix} w_1 \\ s_1 \\ w_2 \\ s_2 \end{Bmatrix}^e = \begin{Bmatrix} f_1 \\ 0 \\ f_2 \\ 0 \end{Bmatrix}^e + \begin{Bmatrix} Q_1 \\ Q_2 \\ Q_3 \\ Q_4 \end{Bmatrix}^e \tag{3.125}$$

Step 5 For convenience, we can write the element stiffness equation (3.125) as

$$[K]^e \{U\}^e = \{F\}^e$$

where $[K]^e$ is the element stiffness matrix, $\{U\}^e$ are generalised element displacements and $\{F\}^e$ the generalised element force vector. We then assemble all the elements to obtain

$$\{F\} = \sum_e \{F\}^e \tag{3.126}$$

$$[K] = \sum_e [K]^e \tag{3.127}$$

Stage 6 In this stage, we introduce the boundary conditions and then solve the system of equations. The composite sandwich beam is simply supported, meaning that only the vertical motion is constrained at the supporting ends. By symmetry, $u\left(L/2, z\right) = z\Psi\left(L/2\right) = 0$. This means $\Psi\left(L/2\right) = 0$ and it is sufficient to solve only half the model. The associated essential boundary conditions are

$$W\left(0\right) = 0;$$

$$\Psi\left(L/2\right) = 0.$$

Stage 7 Once the displacements have been solved, the results are normalised using the following transformation.

$$w_i^* = \frac{w_i}{L} \tag{3.128}$$

$$f_i^* = \frac{f_i}{F} \tag{3.129}$$

where L is the beam length as mentioned before and F is the maximum force under investigation. In this study, $F = 400N$. The maximum normalised displacement is then extracted. This analysis is then repeated for a variety of loads and the associated normalised displacement-load graph plotted.

To solve the finite element model outlined above, we implemented the numerical algorithm discussed in steps 1-6 in MATLAB. The program is available on the accompanying CD under the folder Program Files\Timoshenko Beam Code.

3.2 Nonlinear analysis

In order to obtain the nonlinear finite element model, we basically repeat the same steps we used to obtain the linear finite element model.

Premultiplying the integral equations (2.82) and (2.83) by v_1 and v_2 respectively, and integrating over the element $\Omega^e = (x_e, x_{e+1})$, we have the following variational forms of the governing equations:

$$\int_{x_e}^{x_{e+1}} v_1 \left\{ \frac{d}{dx}\left(\frac{EA}{2}\left(\frac{dW}{dx}\right)^2 \right) + \frac{d}{dx}\left(GAK\left(\frac{dW}{dx}+\Psi\right)\right) + f \right\} dx = 0 \tag{3.130}$$

$$\int_{x_e}^{x_{e+1}} v_2 \left\{ \frac{d}{dx}\left(EI\frac{d\Psi}{dx}\right) - GAK\left(\frac{dW}{dx}+\Psi\right)\right\} dx = 0 \tag{3.131}$$

Distributing the derivative evenly between the field variables and test functions by integrating by parts results in the following variational form

$$\int_{x_e}^{x_{e+1}} \left\{ \frac{d\left(v_1\right)}{dx}\left(\frac{EA}{2}\left(\frac{dW}{dx}\right)^2 + GAK\left(\frac{dW}{dx}+\Psi\right)\right) - f\delta v_1 \right\} dx = \left[\left(Q_x + N_{xx}\frac{dW}{dx}\right) v_1 \right]_{x_e}^{x_{e+1}} \tag{3.132}$$

$$\int_{x_e}^{x_{e+1}} \left\{ \frac{d\left(v_2\right)}{dx}\left(EI\frac{d\Psi}{dx}\right) + GAK\left(\frac{dW}{dx}+\Psi\right) v_2 \right\} dx = \left[M_{xx} v_2 \right]_{x_e}^{x_{e+1}} \tag{3.133}$$

As in the linear model, we introduce the following boundary terms for convenience

$$-\left(Q_x + N_{xx}\frac{dW}{dx}\right)|_{x_e} = \widehat{Q}_1^e \qquad \left(Q_x + N_{xx}\frac{dW}{dx}\right)|_{x_{e+1}} = \widehat{Q}_3^e \tag{3.134}$$

and

$$-EI\frac{d\Psi}{dx}|_{x_e} = Q_2^e \qquad EI\frac{d\Psi}{dx}|_{x_{e+1}} = Q_4^e \tag{3.135}$$

Once again, the equal-order reduced integration approach was followed using linear Lagrange interpolating functions for both W and Ψ.

Substitution of the linear interpolating functions of W and ψ into equations (3.132) and (3.133) and then collecting like terms gives

$$\sum_{j=1}^{2} K_{ij}^{11} w_j + \sum_{j=1}^{2} K_{ij}^{12} s_j = F_i^1 \tag{3.136}$$

$$\sum_{j=1}^{2} K_{ij}^{21} w_j + \sum_{j=1}^{2} K_{ij}^{22} s_j = F_i^2 \tag{3.137}$$

where

$$K_{ij}^{11} = \int_{x_e}^{x_{e+1}} \left(\frac{EA}{2} \left(\frac{dW}{dx} \right)^2 \frac{d\psi_i^{(1)}}{dx} \frac{d\psi_j^{(1)}}{dx} + GAK \frac{d\psi_i^{(1)}}{dx} \frac{d\psi_j^{(1)}}{dx} \right) dx \tag{3.138}$$

$$K_{ij}^{12} = \int_{x_e}^{x_{e+1}} GAK \frac{d\psi_i^{(1)}}{dx} \psi_j^{(2)} dx = K_{ji}^{21} \tag{3.139}$$

$$K_{ij}^{22} = \int_{x_e}^{x_{e+1}} \left(EI \frac{d\psi_i^{(2)}}{dx} \frac{d\psi_j^{(2)}}{dx} + GAK \psi_i^{(2)} \psi_j^{(2)} \right) dx \tag{3.140}$$

$$F_i^1 = \int_{x_e}^{x_{e+1}} f \psi_i^{(1)} dx + \widehat{Q}_{2i-1}^e \tag{3.141}$$

$$F_i^2 = \widehat{Q}_{2i}^e \tag{3.142}$$

As in the linear finite element model, the associated element equations are given by

$$\begin{bmatrix} [K^{11}] & [K^{12}] \\ [K^{21}] & [K^{22}] \end{bmatrix} \begin{Bmatrix} \{w\} \\ \{s\} \end{Bmatrix} = \begin{Bmatrix} \{F^1\} \\ \{F^2\} \end{Bmatrix} \tag{3.143}$$

The nonlinear finite element model differs from its linear counterpart in that the global stiffness matrix now depends on the unknown solution. To see this, one need only compare equation (3.114) with equation (3.138). A number of techniques for solving nonlinear finite element methods exist of which the easiest is the direct iteration or Picard's method [REDDY, 1993]. In this study, we shall however employ the Newton's or Newton-

Raphson's method. To develop the Newton-Raphson technique, we define $\{\Delta\}$, the generalised displacements, as

$$\{\Delta\} = \begin{Bmatrix} \{w\} \\ \{s\} \end{Bmatrix} \tag{3.144}$$

and therefore $\{\Delta\}^r$ represents the displacement solution at the rth iteration. We can write equation (3.143) as

$$[K(\{\Delta\})]\{\Delta\} = \{F\} \tag{3.145}$$

Define the residual, $\{R\}$, as

$$\{R\}(\{\Delta\}) \equiv [K(\{\Delta\})]\{\Delta\} - \{F\} = 0 \tag{3.146}$$

resulting in the following residual at the rth iteration

$$\{R\}^r = \left[K^T(\{\Delta\}^r)\right]\{\Delta\}^r - \{F\} \tag{3.147}$$

then expanding $\{R\}$ in Taylor's series about $\{\Delta\}^r$, we obtain [REDDY, 2004]

$$\begin{aligned} 0 &= \{R\}^r + \left[\frac{\partial\{R\}}{\partial\{\Delta\}}\right]^r \left(\{\Delta\}^{r+1} - \{\Delta\}^r\right) \\ &\quad + \frac{1}{2!}\left[\frac{\partial^2\{R\}}{\partial\{\Delta\}\,\partial\{\Delta\}}\right]^r \left(\{\Delta\}^{r+1} - \{\Delta\}^r\right)^2 + \ldots \end{aligned} \tag{3.148}$$

or

$$0 = \{R\}^r + \left(\left[K^T(\{\Delta\}^r)\right]\right)\{\delta\Delta\}^r + O\left(\{\delta\Delta\}^2\right) \tag{3.149}$$

where $\{\delta\Delta\}^r = \{\Delta\}^{r+1} - \{\Delta\}^r$, $O(\cdot)$ denotes the higher-order terms in $\{\delta\Delta\}$, and $\left[K^T\right]$ is known as the tangent stiffness matrix [REDDY, 2004] defined by

$$\left[K^T(\{\Delta\}^r)\right] = \left[\frac{\partial\{R\}}{\partial\{\Delta\}}\right]^r \tag{3.150}$$

To solve the nonlinear finite element equations, compute the element tangent stiffness matrices and residual vectors using equations (3.147) and (3.150), then assemble the global

tangent stiffness matrix and residual force vector. Finally solve the assembled equations for the incremental displacement vector after imposing the boundary conditions of the problem.

Neglecting higher order terms in equation (3.149), we obtain, after rearranging

$$\{\delta\Delta\}^r = -\left[K^T\left(\{\Delta\}^r\right)\right]^{-1}\{R\}^r \tag{3.151}$$

from where the total displacement vector can be obtained as

$$\{\Delta\}^{r+1} = \{\Delta\}^r + \{\delta\Delta\}^r \tag{3.152}$$

Assuming that $\{\Delta\}^0 = \{0\}$, that is, the first iteration is a linear one, we use the solution we obtain to calculate the total displacement vector of the first iteration. We carry out the iteration process until the difference between $\{\Delta\}^r$ and $\{\Delta\}^{r+1}$ has reduced to a prescribed error tolerance. The convergence criteria to terminate the iterations is based on the magnitude of the displacement increments and is given as [BELYTSCHKO et al., 2000]

$$\frac{\|\{\delta\Delta\}^r\|}{\left\|\{\Delta\}^{r+1}\right\|} < \epsilon \tag{3.153}$$

Generally, convergence of the Newton-Raphson method is conditional, meaning it is dependent on the value on the initial guess. However, by starting with a linear approximation to the solution ensures that the scheme is unconditionally stable since a linear solution already exists. The iterative solution either stays linear or converges to some other stable nonlinear solution, within the prescribed error tolerance.

3.2.1 Calculating the Element Tangent Stiffness Coefficients

Rearranging equation (3.149) after neglecting $O\left(\{\delta\Delta\}^2\right)$ yields

$$\left(\left[K^T\left(\{\Delta\}^r\right)\right]\right)\{\delta\Delta\}^r = -\{R\}^r \tag{3.154}$$

Since $\delta\Delta_i^1 = w_i$ and $\delta\Delta_i^2 = s_i$, the Newton-Raphson method can be written in the form

$$\begin{bmatrix} [T^{11}] & [T^{12}] \\ [T^{21}] & [T^{22}] \end{bmatrix}^r \begin{Bmatrix} \{\delta\Delta^1\} \\ \{\delta\Delta^2\} \end{Bmatrix}^r = -\begin{Bmatrix} \{R^1\} \\ \{R^2\} \end{Bmatrix}^r \tag{3.155}$$

where the components of the submatrices $\left[T^{\alpha\beta}\right]$ are defined by

$$T_{ij}^{\alpha\beta} = \frac{\partial R_i^\alpha}{\partial \Delta_j^\beta} \tag{3.156}$$

and the components of the residual vector are given by

$$R_i^\alpha = \sum_{\gamma=1}^{2}\sum_{k=1}^{2} K_{ik}^{\alpha\gamma}\Delta_k^\gamma - F_i^\alpha \tag{3.157}$$

Thus from equation (3.156) we have

$$T_{ij}^{\alpha\beta} = \frac{\partial}{\partial \Delta_j^\beta}\left(\sum_{\gamma=1}^{2}\sum_{k=1}^{2} K_{ik}^{\alpha\gamma}\Delta_k^\gamma - F_i^\alpha\right) \tag{3.158}$$

$$= \sum_{\gamma=1}^{2}\sum_{k=1}^{2} \frac{\partial K^{\alpha\gamma}}{\partial \Delta_j^\beta}\Delta_k^\gamma + K_{ij}^{\alpha\beta} \tag{3.159}$$

Since the only coefficient depending on the solution is K_{ij}^{11} and is a function of $\Delta_i^1 = w_i$, the derivatives of all stiffness coefficients with respect to $\Delta_i^2 = s_i$ are zero so that

$$T_{ij}^{11} = \sum_{\gamma=1}^{2}\sum_{k=1}^{2} \frac{\partial K_{ik}^{1\gamma}}{\partial w_j}\Delta_k^\gamma + K_{ij}^{11} = \sum_{k=1}^{2} \frac{\partial K_{ik}^{11}}{\partial w_j} w_k + K_{ij}^{11} \tag{3.160}$$

$$\sum_{k=1}^{2} \frac{\partial K_{ik}^{11}}{\partial w_j} w_k = \frac{1}{2}\sum_{k=1}^{2} w_k \frac{\partial}{\partial w_j}\left[\int_{x_e}^{x_k}\left\{EA\left(\frac{dW}{dx}\right)^2 \frac{d\psi_i^{(1)}}{dx}\frac{d\psi_j^{(1)}}{dx} + GAK\frac{d\psi_i^{(1)}}{dx}\frac{d\psi_j^{(1)}}{dx}\right\}dx\right] \tag{3.161}$$

resulting in

$$\sum_{k=1}^{2} \frac{\partial K_{ik}^{11}}{\partial w_j} w_k = \int_{x_e}^{x_{e+1}} \left\{ EA \left(\frac{dW}{dx} \right)^2 \frac{d\psi_i^{(1)}}{dx} \frac{d\psi_j^{(1)}}{dx} \right\} dx \tag{3.162}$$

finally resulting in

$$T_{ij}^{11} = \int_{x_e}^{x_{e+1}} \left\{ EA \left[\frac{3}{2} \left(\frac{dW}{dx} \right)^2 \right] \frac{d\psi_i^{(1)}}{dx} \frac{d\psi_j^{(1)}}{dx} + GAK \frac{d\psi_i^{(1)}}{dx} \frac{d\psi_j^{(1)}}{dx} \right\} dx \tag{3.163}$$

Since K_{ij}^{12}, K_{ij}^{21} and K_{ij}^{22} do not depend on the unknown solution, their derivatives with respect to $\Delta_i^1 = w_i$ are identically zero and it can be easily shown that

$$T_{ij}^{12} = K_{ij}^{12} \tag{3.164}$$

$$T_{ij}^{21} = K_{ij}^{21} \tag{3.165}$$

$$T_{ij}^{22} = K_{ij}^{22} \tag{3.166}$$

Besides T_{ij}^{11}, all the other coefficients of the tangent stiffness matrix can be deduced directly from the element stiffness matrix for the linear finite element model. Calculation of T_{ij}^{11} is indicated below, but all other terms will be assumed from earlier calculations. Once again

$$W = \psi_1^{(1)} w_1 + \psi_1^{(2)} w_2 \tag{3.167}$$

$$W = \frac{x_{e+1} - x}{l} w_1 + \frac{x - x_e}{l} w_2 \tag{3.168}$$

so that

$$\left(\frac{dW}{dx} \right)^2 = \left(\frac{w_2 - w_1}{l} \right)^2 \tag{3.169}$$

Thus, from equation (3.163) , using the transformation $x = x_e + \frac{l}{2}(\xi + 1)$ yields

$$T_{11}^{11} = \int_{-1}^{1} \left(\frac{3EA}{2} \left(\frac{w_2 - w_1}{l} \right)^2 \left(-\frac{1}{l} \right)^2 \right) \frac{l}{2} d\xi \tag{3.170}$$

$$+ \int_{-1}^{1} GAK \left(\frac{1}{l} \right)^2 \left(\frac{l}{2} d\xi \right) \tag{3.171}$$

$$T_{11}^{11} = \frac{3EA\left(w_2 - w_1\right)^2}{l^3} + \frac{GAK}{l} \tag{3.172}$$

Similarly, we can calculate T_{12}^{11}, T_{21}^{11} and T_{22}^{11}:

$$\left[T^{11}\right] = \frac{3EA\left(w_2 - w_1\right)^2}{2l^3} \begin{bmatrix} 1 & -1 \\ -1 & 1 \end{bmatrix} + \frac{GAK}{l} \begin{bmatrix} 1 & -1 \\ -1 & 1 \end{bmatrix} \tag{3.173}$$

$$\left[T^{11}\right] = \left(\frac{3EA\left(w_2 - w_1\right)^2}{2l^3} + \frac{GAK}{l} \right) \begin{bmatrix} 1 & -1 \\ -1 & 1 \end{bmatrix} \tag{3.174}$$

This completes the derivation of the element tangent stiffness matrix. Substituting for the tangent stiffness coefficients in equation (3.163) and rearranging gives the following equation of element Ω^e at the rth iteration.

$$\begin{bmatrix} \frac{3EA(w_2-w_1)^2}{2l^3} + \frac{GAK}{l} & -\frac{GAK}{2} & -\frac{3EA(w_2-w_1)^2}{2l^3} - \frac{GAK}{l} & -\frac{GAK}{2} \\ -\frac{GAK}{2} & \frac{EI}{l} + \frac{GAKl}{4} & \frac{GAK}{2} & \frac{GAKh}{4} - \frac{EI}{l} \\ -\frac{3EA(w_2-w_1)^2}{2l^3} - \frac{GAK}{l} & \frac{GAK}{2} & \frac{3EA(w_2-w_1)^2}{2l^3} + \frac{GAK}{l} & \frac{GAK}{2} \\ -\frac{GAK}{2} & \frac{GAKl}{4} - \frac{EI}{l} & \frac{GAK}{2} & \frac{EI}{l} + \frac{GAKl}{4} \end{bmatrix}_e^r \begin{Bmatrix} \delta w_1 \\ \delta s_1 \\ \delta w_2 \\ \delta s_2 \end{Bmatrix}_e^r = - \begin{Bmatrix} R^1 \\ 0 \\ R^2 \\ 0 \end{Bmatrix}_e^r \tag{3.175}$$

Finally, the element equations are assembled, the boundary conditions enforced and the resulting global equations solved iteratively.

A MATLAB based program implementing this algorithm was developed and is available on the accompanying CD under the folder Program Files\Timoshenko Beam Code. The numerical experiment was then repeated for a variety of loads and a graph of the load-maximum load was then plotted.

3.3 Experimental Analysis

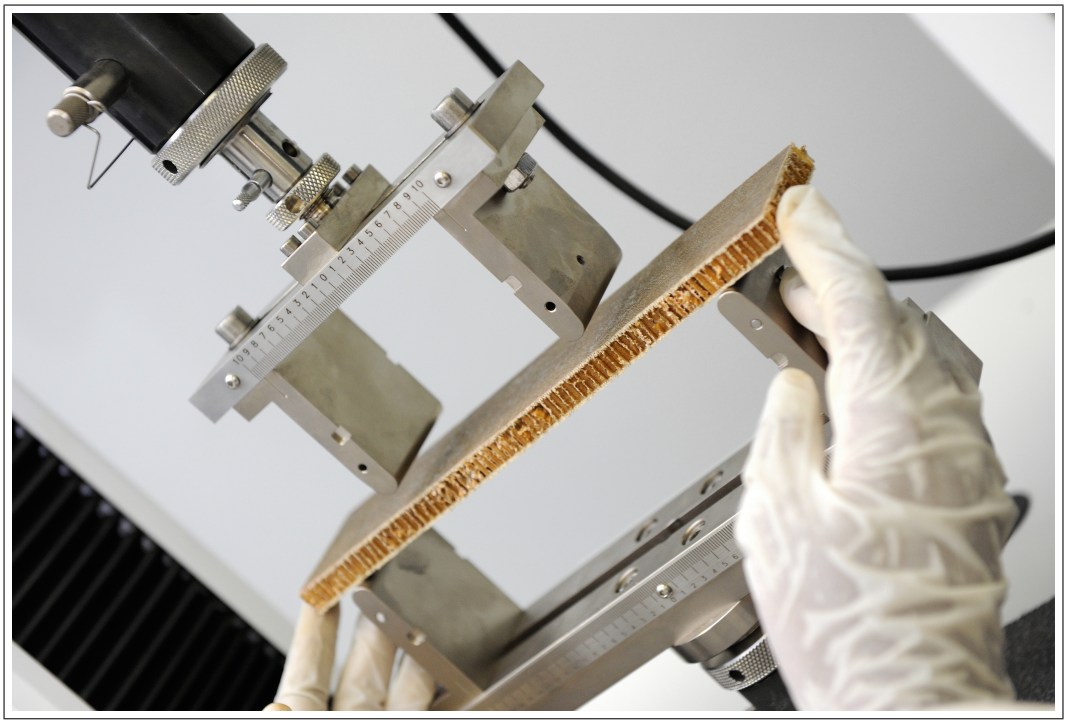

Fig. 3.4. Four point bending apparatus at the CSIR Research Facilities, Summerstrand, Port Elizabeth

To validate the numerical model, four-point bending experiments were carried out on the composite sandwich beams at the CSIR Research facilities in Summerstrand, Port Elizabeth with the help of Dr. Maya John. The apparatus used to carry out the four-point bending experiments is shown in Fig(3.4) .

The CSIR developed the composite sandwich beams using Nomex honeycomb cores provided by AIRBUS and resin-filled natural fibre woven fabric acquired from Libeco Group of Companies in Belgium.

The material properties and dimensions of the composite sandwich beam supplied by Dr. Maya John from the CSIR are summarised below

- Core properties

$$E_{xx} = 15\text{MPa} \tag{3.176}$$

$$G_{xz} = 0.45\text{MPa} \tag{3.177}$$

$$\text{thickness} = 9.45\text{mm} \tag{3.178}$$

- Facesheet properties

$$E_{xx} = 1000\text{MPa} \tag{3.179}$$

$$G_{xz} = 500\text{MPa} \tag{3.180}$$

$$\text{thickness} = 0.65\text{mm} \tag{3.181}$$

- Sandwich panel dimensions

$$\text{Span of panel} = 190\text{mm} \tag{3.182}$$

$$\text{Width of span} = 50\text{mm} \tag{3.183}$$

Compared to three point flexure, four point flexure has the advantage of a distributed centre load which avoids local stress concentrations observed in three point flexure experiment [WHITNEY and BROWNING, 1985]. The specimen was loaded at a rate of 12mm/min.

3.4 Results and discussion

The normalised load-displacement curves from the numerical and experimental analysis were plotted on the same graph and are shown in Fig (3.5) .

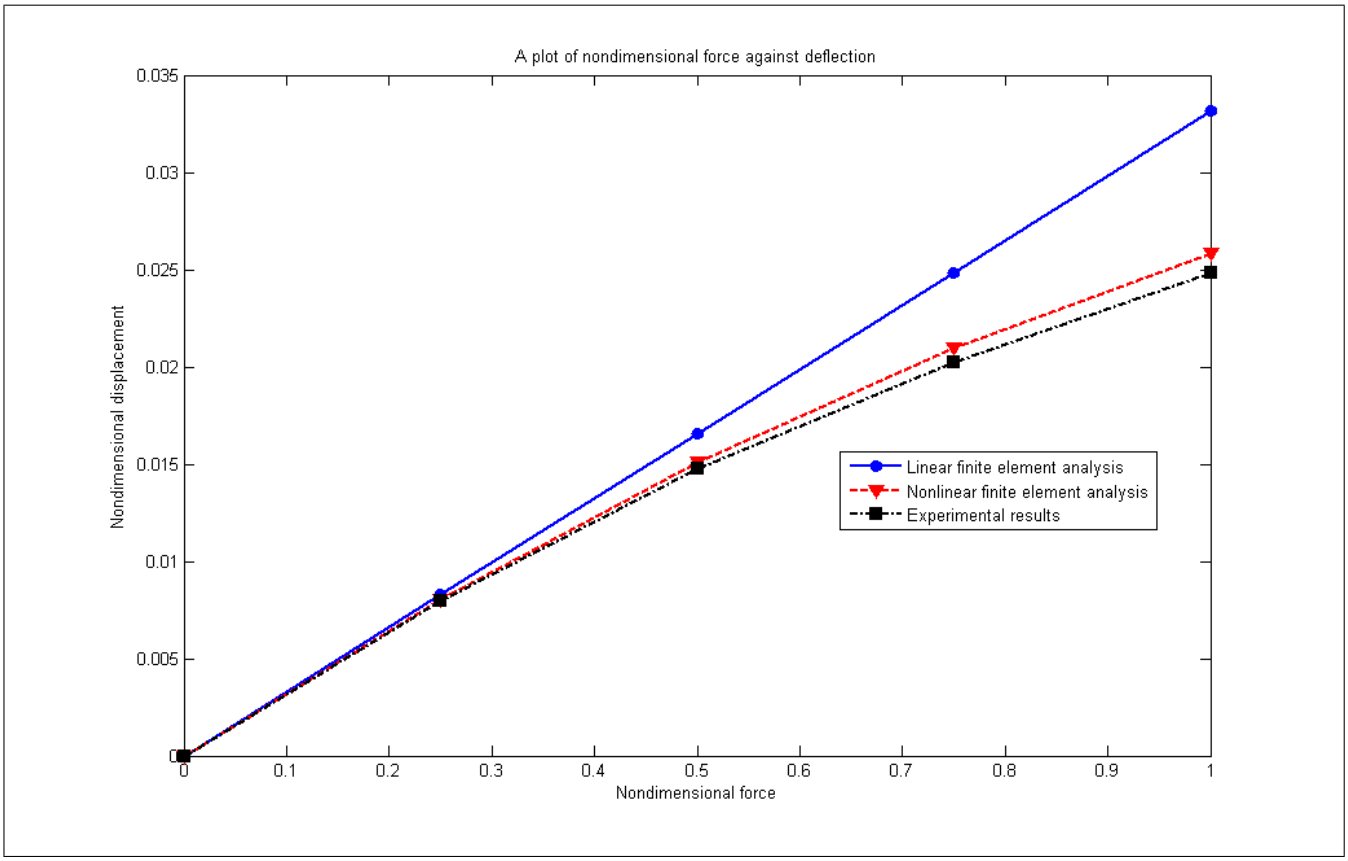

Fig. 3.5. Force-displacement diagram

The nonlinear finite element analysis starts linearly before becoming nonlinear because of geometric nonlinearity. In geometric nonlinearity, the composite sandwich beam becomes shorter as it bends. For large deformations, the linear finite element analysis gives higher displacements than those obtained from nonlinear analysis. The nonlinear solution

compares well with experimental results though the difference between the nonlinear solution and the experimental result becomes more nonlinear as the load increases. Another possible reason may also be the material nonlinearity of the core, which we have not factored in the model. Further, as the load increases, the hollows structure starts to crumble inwards around the loading pins possibly resulting in a lower observed deflection of the composite sandwich beam.

Chapter 4
Delamination Modelling

Earlier, core-facesheet delamination was identified as one of the failure mechanisms present in composite sandwich structures [MEO et al., 2003]. Despite its obvious benefits, delamination modelling remains complex. Traditionally, modelling delamination required the introduction of two models, namely, initiation of delamination and fracture mechanics. This two-pronged approach has been eliminated by the introduction of a single so-called cohesive zone model. The cohesive zone model has been employed to numerically investigate the behaviour of a repaired composite sandwich beam subjected to four-point bending [RAMANTANI et al., 2010]. The researchers investigated the numerical model using the finite element software package ABAQUS to study overlap and scarf repairs and were able to draw useful results on the influence of several geometrical parameters, such as overlap length and patch thickness for overlap repairs and scarf angle for scarf repairs.

This chapter will review the cohesive zone model with the view to laying a foundation for the numerical study presented in the next chapter. Delamination will be reviewed from a three dimensional perspective as reduction to two dimensions follows naturally.

4.1 Cohesive zone modelling

In cohesive zone models, the interface or the region where delamination might occur is replaced with a cohesive or damage zone. The interface is then modelled by relating tractions across the interface to the separation of the interface [ZOU et al., 2003]. The basic

assumption is that all the delamination occurs in the interface. Numerically, the cohesive zone can be represented by nonlinear spring elements [MEO et al., 2003], continuum damage interface elements [ZOU et al., 2003], or decohesion interface elements. The last mentioned have proved popular among researchers analysing delamination in composite materials [REEDY et al., 1997, DAVILA et al., 2001].

The delamination process comprises two stages, namely

- delamination initiation
- delamination propagation or growth

For a composite sandwich structure, we assume that delamination occurs in the interface between the core and the facesheet. We relate the interlaminar tractions in the interface to the separation of the two layers at the interface and determine the delamination initiation by the interlaminar strength of the interface. Interface tractions initially increase with increasing separation of the interface until they reach a maximum beyond which they begin to diminish and then eventually vanish for a certain maximum displacement determined by the interface traction-relative displacement relations. One standard traction-relative displacement relation is the bilinear model proposed by REEDY et al. (1997). Interlaminar tractions consist of interlaminar normal tractions and the interlaminar shear tractions giving rise to various modes of delamination. There are three basic modes of delamination deformation, [GIBSON, 2007] namely

1. Mode I - opening of a delamination,
2. Mode II - in-plane shear of delamination or the sliding mode, and

3. Mode III - anti-plane shear of a delamination or scissoring mode.

In a mode I delamination, a tensile force will be acting normal to the plane of the delamination. In a mode II delamination, a shear stress will be acting parallel to the plane of the delamination and perpendicular to the delamination front whereas in a mode III delamination, a shear stress will be acting parallel to the plane of the delamination and perpendicular to the delamination front.

The application of the bilinear model to a single delamination mode is rather straightforward, however, mode interactions must be considered in the case of mixed-mode interactions [ZOU et al., 2003]. In 1998, MI et al. used the bilinear model to simulate delamination in fibre composites, using decohesion interface elements to represent the cohesive zone. They also developed numerical solutions for the Double Cantilever Beam test, the End Notched Flexure test, and the Mixed Mode Bending test. Using a similar approach, DAVILA et al. (2001) formulated and implemented the bilinear model in ABAQUS using a single displacement-based damage variable. They tested the accuracy of their method against analytical solutions obtained by MI et al. (1998). Mixed-mode decohesion interface elements were implemented in ANSYS by JIANG et al. (2005) to study the effects of size on the strength of a series of carbon-fibre epoxy specimens. IVANEZ et al. (2010) used the finite element analysis package ABAQUS to analyse the bending behaviour of a composite sandwich beam with foam core subjected to three-point loading. They went further also for modelling the impact behaviour. Their numerical results compared favourably with experimental. Delamination was one of the failure modes they included though they did not explain the methods used in their analysis.

Stress-based failure techniques are suitable for predicting the onset of delamination. A popular stress based technique for predicting onset of delamination is the Brewer and Lagace Quadratic Stress Criterion [BREWER and LAGACE, 1988] which is defined by

$$\left(\frac{\sigma_{zz}}{T}\right)^2 + \left(\frac{\tau_{yz}}{S_{yz}}\right)^2 + \left(\frac{\tau_{xz}}{S_{xz}}\right)^2 \geq 1 \quad \text{if} \quad \sigma_{zz} > 0 \tag{4.184}$$

or

$$\left(\frac{\tau_{yz}}{S_{yz}}\right)^2 + \left(\frac{\tau_{xz}}{S_{xz}}\right)^2 \geq 1 \quad \text{if} \quad \sigma_{zz} < 0 \tag{4.185}$$

for an initially intact surface where

$$T = \text{ tensile interlaminar normal strength,}$$

$$S_{yz} = \text{ interlaminar shear strength for } \tau_{yz} \text{ stress and}$$

$$S_{xz} = \text{ interlaminar shear strength for } \tau_{xz} \text{ stress.}$$

The Brewer and Lagace Quadratic Stress Criterion only considers tensile normal stresses for delamination since direct compressive normal stresses do not contribute to the initiation of delamination.

The cohesive zone modelling technique for delamination employs the best of both worlds by using the stress states to predict delamination and then using fracture mechanics indirectly to capture the delamination growth. In this study, the following traction displacement constitutive relationship to model the cohesive zone interface [ZOU et al., 2002] will be applied

$$\sigma_{zz} = k_1\delta_{v_z} = kT\delta_{v_z} \tag{4.186}$$

$$\tau_{xz} = k_2\delta_{v_x} = kS_{xz}\delta_{v_x} \tag{4.187}$$

$$\tau_{yz} = k_3\delta_{v_y} = kS_{yz}\delta_{v_y} \tag{4.188}$$

where

$$\begin{aligned}
\sigma_{zz} &= \text{interlaminar normal stress} \\
\delta_{v_x}, \delta_{v_y}, \delta_{v_z} &= \text{relative displacement components across the interface} \\
k &= 10^4 \text{ - } 10^7 \text{mm}^{-1} \\
k_1, k_2, k_3 &= \text{penalty stiffness parameters where} \\
k_1 &= kT \\
k_2 &= kS_{xz} \\
k_3 &= kS_{yz}
\end{aligned}$$

Employing equations (4.186) , (4.187) and (4.188) , it can be easily seen that

$$\sqrt{\sigma_{zz}^2 + \tau_{xz}^2 + \tau_{yz}^2} = kT\sqrt{\delta_{v_z}^2 + \beta_1^2\delta_{v_x}^2 + \beta_2^2\delta_{v_y}^2} \tag{4.189}$$

simplifying to

$$\sigma = kT\delta_v = k_1\delta_v \tag{4.190}$$

where

$$\beta_1 = \frac{S_{xz}}{T} \qquad \beta_2 = \frac{S_{yz}}{T} \tag{4.191}$$

$$\sigma = \sqrt{\sigma_z^2 + \tau_{xz}^2 + \tau_{yz}^2} = \text{effective stress and} \tag{4.192}$$

$$\delta_v = \sqrt{\delta_{v_z}^2 + \beta_1^2\delta_{v_x}^2 + \beta_2^2\delta_{v_y}^2} = \text{effective displacement} \tag{4.193}$$

The traction-displacement relationship for the effective stress-effective displacement is a three dimensional or mixed-mode delamination relation [MSC.Software, 2007]. Thus for a mixed-mode delamination, the following relationship holds

$$\sigma = k_1\delta_v \tag{4.194}$$

4.1.1 The penalty stiffness parameter

Choosing a value for the penalty stiffness parameter requires experience. Choosing a small value for the penalty stiffness parameter results in large interpenetrations [de MOURA et al., 1997] resulting in inaccurate modelling of physical reality whereas choosing a very high value results in numerical errors related to computer precision. The two most commonly used methods for determining the penalty stiffness parameters are

1. Using the elastic shear moduli of the interface material, [DAVILA et al., 2001, MEO and THIEULOT, 2005, REEDY et al., 1997] and

2. Using interlaminar strengths [ZOU et al., 2002].

Researchers use different values for the interface penalty stiffness, 2×10^3mm^{-1} and 1×10^4mm^{-1} for the normal and shear penalty stiffness, respectively [REEDY et al., 1997]; and other values given in literature [SCHELLEKENS and de BORST, 1991, MI et al., 1998, GONCALVES et al., 2000] ranged from 1×10^7 to 1×10^8mm^{-1}.

In 2001, DAVILA et al. went further to suggest an optimum value of 1×10^6 after conducting a series of experiments. This condition was relaxed by ZOU et al.(2002) who generalised the value for the penalty stiffness parameter to $k = 1 \times 10^4 \sim 1 \times 10^7$mm^{-1}. Any value lying within the range suggested by ZOU et al.(2002) should satisfy the twin objectives of satisfying the interface continuity conditions and making sure that there are no numerical errors due to ill-conditioning and unnecessarily long runtime. The use of the

interlaminar strengths allows the use of the penalty stiffness value to determine directly the maximum effective displacement at delamination initiation.

4.2 Bilinear softening model

There are different models available in literature to model the traction-displacement relation. A review of these traction-displacement curves is available in ZOU et al. (2003) and some of which are cubic/exponential [NEEDLEMAN, 1987, XU and NEEDLEMAN, 1994], bilinear [REEDY et al., 1997, MI et al., 1998], perfectly plastic [CUI and WISNOM, 1993] and trapezoidal [TVERGAARD and HUTCHINSON, 1992]. For simplicity, in this study will use the bilinear model or the bilinear softening model to model the traction-displacement relation.The bilinear softening model is a standard cohesive zone model proposed by DAVILA et al. (2001) in which stress-displacement behaves as shown in Fig (4.6) [REEDY et al., 1997, MEO and THIEULOT, 2005].

The curve in Fig (4.6) is divided into 3 regions,

Region 1 elastic damage region, $0 \leq \delta_v < \delta_{v_{crit}}$;

Region 2 softening region, $\delta_{v_{crit}} \leq \delta_v < \delta_{v_{\max}}$;

Region 3 decohesion region, $\delta_v \geq \delta_{v_{\max}}$,

where $\delta_{v_{crit}}$ is the value of the displacement which corresponds to the maximum tractions across the interface and $\delta_{v_{\max}}$ is the value the displacement which corresponds to the value when the interface material is completely damaged.

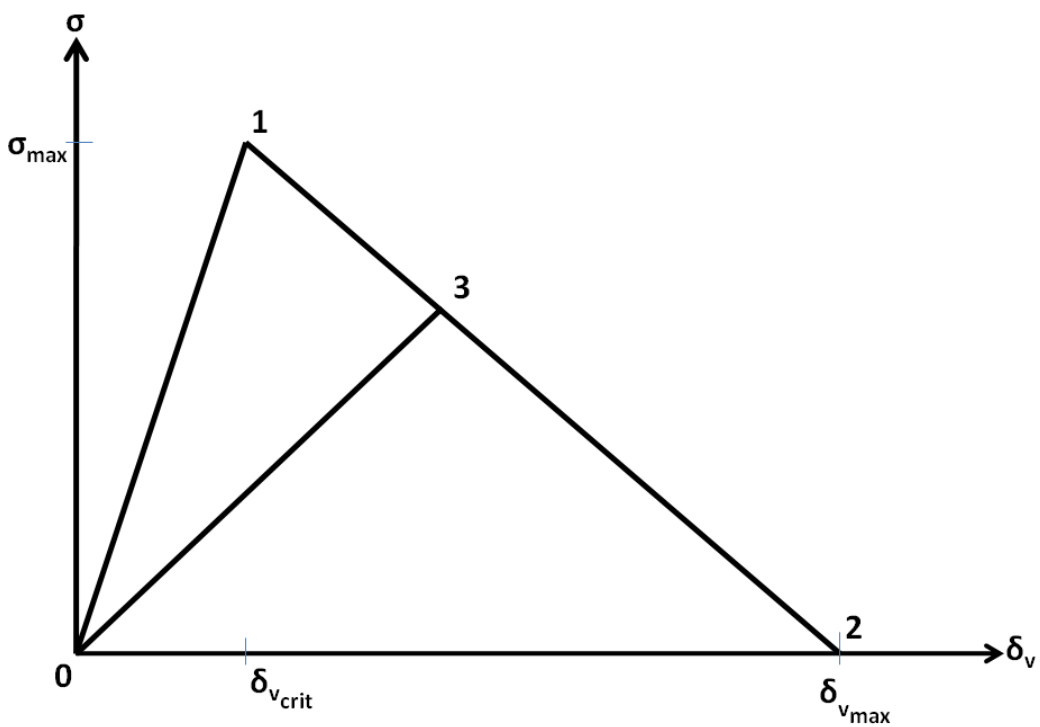

Fig. 4.6. Bilinear softening model

In the elastic region, the stress-displacement relationship is given by

$$\sigma = k_1 \delta_v \tag{4.195}$$

while in the softening region, it is given by

$$\sigma = (1 - d)\, k_1 \delta_v, \quad 0 \leq d \leq 1 \tag{4.196}$$

where the variable d represents the accumulated damage, which is equal to zero in the undamaged state and unity in the fully damaged state. Equation (4.196) shows that as the damage increases in the softening region, the effective traction, σ, decreases. The tractions becomes zero when $\delta_v = \delta_{v_{\max}}$ and so for $\delta_v \geq \delta_{v_{\max}}$, there is complete separation of the neighbouring layers.

4.2.1 Delamination initiation

From the Brewer-Lagace Quadratic Failure Criterion for the initiation of delamination, we have

$$\left(\frac{\sigma_{zz}}{T}\right)^2 + \left(\frac{\tau_{xz}}{S_{xz}}\right)^2 + \left(\frac{\tau_{yz}}{S_{yz}}\right)^2 = 1. \tag{4.197}$$

From equations (4.186) , (4.187) and (4.188) we obtain

$$(\delta_{v_z})^2 + (\delta_{v_x})^2 + \left(\delta_{v_y}\right)^2 = \frac{1}{k^2}. \tag{4.198}$$

then clearly

$$(\delta_{v_z})^2 \leq (\delta_{v_z})^2 + (\delta_{v_x})^2 + \left(\delta_{v_y}\right)^2 = \frac{1}{k^2} \tag{4.199}$$

resulting in

$$\delta_{v_z} \leq \frac{1}{k} \text{ provided that } \delta_{v_z} \geq 0$$

We now assume that the displacements δ_{v_x}, δ_{v_y} and δ_{v_z}, satisfy the condition:

$$\max\left(\delta_{v_x}, \delta_{v_y}, \delta_{v_z}\right) = \frac{1}{k}. \tag{4.200}$$

which is, in fact, a stronger condition than that given by ZOU et al. (2002) . Now, using this condition in equation (4.200) , we can define the maximum or critical displacement before damage initiation, $\delta_{v_{crit}}$ as

$$\delta_{v_{crit}} = \frac{1}{k}\sqrt{1 + \beta_1^2 + \beta_2^2}$$

Now employing equations (4.191) and (4.192) , we can define the maximum effective stress as

$$\sigma = \sqrt{\sigma_{zz}^2 + \tau_{xz}^2 + \tau_{yz}^2}. \tag{4.201}$$

in terms of the interlaminar normal stress, T, and interlaminar shear stress, S, so that

$$\sigma = k_1 \delta_v \tag{4.202}$$

resulting in

$$\sigma_{\max} = k_1 \delta_{v_{crit}} \tag{4.203}$$

further resulting in

$$\delta_{v_{crit}} = \frac{\sqrt{1 + \beta_1^2 + \beta_2^2}}{k} \tag{4.204}$$

Therefore, for a 3D cohesive interface zone model, damage initiates when δ_v reaches $\delta_{v_{crit}}$ given above.

4.2.2 Delamination Propagation

Fracture energy is necessary for delamination propagation and must be supplied to the crack tip [ZOU et al., 2003]. This energy is absorbed by the irreversible damage of the interface

as measured by the damage variable, d. This fracture energy is given by

$$G = \int_0^{\delta v} \sigma d\delta v \tag{4.205}$$

which is the area under the entire curve of the effective strain-effective displacement curve. And so equivalently from an energy point of view, debonding of the two layers is complete when

$$G \geq G_{crit} \tag{4.206}$$

where G_{crit} is the critical fracture energy release rate. From Fig (4.6), we have

$$G_{crit} = \text{ Area of } \Delta 012 = \frac{1}{2} \cdot \delta_{v_{\max}} \cdot \sigma_{\max} \tag{4.207}$$

from which we get

$$\delta_{v_{\max}} = 2 \cdot \frac{G_{crit}}{\sigma_{\max}} \tag{4.208}$$

For pure Mode I delamination, the constitutive relations are:

$$\sigma_{zz} = kT\delta_{v_z} \quad \text{for} \quad 0 \leq \delta_{v_z} < \delta_{v_{z_{crit}}} \tag{4.209}$$

$$\sigma_{zz} = (1-d)\, kT\delta_{v_z} \quad \text{for} \quad \delta_{v_{z_{crit}}} \leq \delta_{v_z} < \delta_{v_{z\max}} \tag{4.210}$$

where the relative z-displacement just before damage initiation, $\delta_{v_{z_{crit}}}$, is given by:

$$\delta_{v_{z_{crit}}} = \frac{T}{kT} = \frac{1}{k}. \tag{4.211}$$

The critical energy release rate for Mode I delamination is given by:

$$G_{1c} = \frac{1}{2}\delta_{v_{z\max}} T. \tag{4.212}$$

The Mode I energy released [DAVILA et al., 2001] is calculated as:

$$G_1 = G_{1c} - \frac{1}{2} \cdot \delta_{v_{z\max}} \cdot \sigma_z = G_{1c} - \frac{1}{2} \cdot \delta_{v_{z\max}} \cdot (1-d)\, kT \cdot \delta_{v_z} \tag{4.213}$$

where, d, the damage parameter is given by:

$$d = \frac{\delta_{v_z} - \delta_{v_{z_{crit}}}}{\delta_{v_{z_{\max}}} - \delta_{v_{z_{crit}}}} \tag{4.214}$$

Substituting equation(4.214) in equation(4.213) , we get

$$G_1 = G_{1c} - \frac{1}{2}\delta_{v_{z_{\max}}} \cdot \delta_{v_z} \cdot kT \left(\frac{\delta_{v_z} - \delta_{v_{z_{\max}}}}{\delta_{v_{z_{crit}}} - \delta_{v_{z_{\max}}}} \right) \tag{4.215}$$

$$\Rightarrow G_1 = G_{1c} - \frac{\delta_{v_{z_{\max}}} kT \cdot \delta_{v_z} \left(\delta_{v_z} - \delta_{v_{z_{\max}}} \right)}{2 \left(\delta_{v_{z_{crit}}} - \delta_{v_{z_{\max}}} \right)}. \tag{4.216}$$

We obtain the Mode II and Mode III energies released by a similar argument as

$$G_{II} = G_{IIC} - \frac{\delta_{v_{x_{\max}}} kS \cdot \delta_{v_x} \left(\delta_{v_x} - \delta_{v_{x_{\max}}} \right)}{2 \left(\delta_{v_{x_{crit}}} - \delta_{v_{x_{\max}}} \right)} \text{ and} \tag{4.217}$$

$$G_{III} = G_{IIIC} - \frac{\delta_{v_{y_{\max}}} kS \cdot \delta_{v_y} \left(\delta_{v_y} - \delta_{v_{y_{\max}}} \right)}{2 \left(\delta_{v_{y_{crit}}} - \delta_{v_{y_{\max}}} \right)}. \tag{4.218}$$

4.3 Interface Element Formulation

This section reviews the cohesive interface element formulation theory [de MOURA et al., 1997, de MOURA et al., 2000, CAMANHO et al., 2003]. The cohesive interface between the facesheet and the core is modelled by the zero-thickness interface element shown in Fig (4.7) A vector of relative displacements between two points having the same relative position can be obtained from the displacement fields of the element faces, top and bottom

$$\delta \underline{U} = \begin{Bmatrix} u \\ v \\ w \end{Bmatrix}_{top} - \begin{Bmatrix} u \\ v \\ w \end{Bmatrix}_{bottom} \tag{4.219}$$

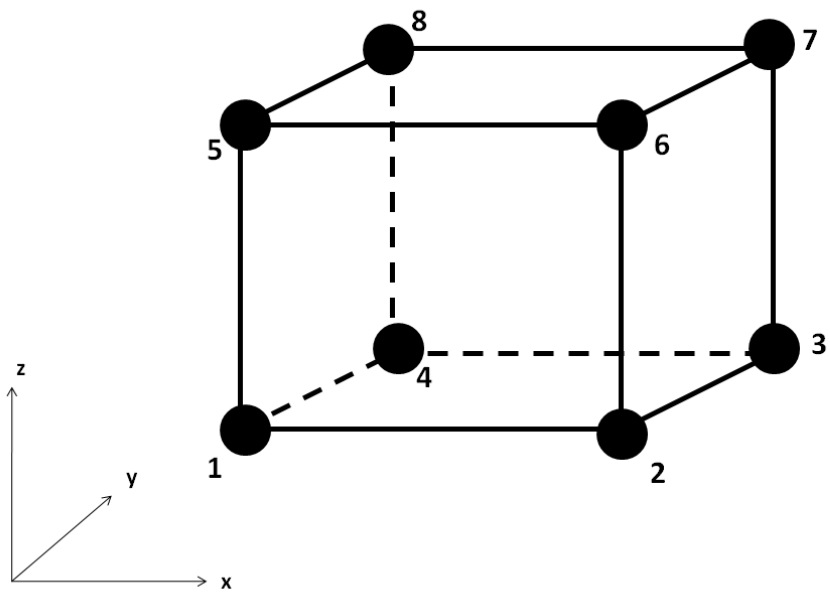

Fig. 4.7. 3D interface element

where u, v and w refer to the normal 3D directions. The displacement field associated with the top face is

$$\begin{Bmatrix} u \\ v \\ w \end{Bmatrix}_{top} = \mathbf{N}_{top}\underline{U}_{top} \tag{4.220}$$

where $\underline{U}$ is the nodal displacement vector

$$\underline{U}_{top} = \begin{Bmatrix} \underline{U}_1 \\ \underline{U}_2 \\ \underline{U}_3 \\ \underline{U}_4 \end{Bmatrix}_{top} \tag{4.221}$$

with

$$\underline{U}_i = \begin{Bmatrix} u_i \\ v_i \\ w_i \end{Bmatrix} \tag{4.222}$$

and

$$\mathbf{N}_{top} = [\mathbf{N}_1, \mathbf{N}_2, \mathbf{N}_3, \mathbf{N}_4]_{top} \tag{4.223}$$

where

$$N_i = \begin{bmatrix} N_i & 0 & 0 \\ 0 & N_i & 0 \\ 0 & 0 & N_i \end{bmatrix} \tag{4.224}$$

The shape of this element are the standard four-noded quadrilateral element. We obtain the bottom relative displacements by a similar argument

$$\begin{Bmatrix} u \\ v \\ w \end{Bmatrix}_{bottom} = \mathbf{N}_{bottom}\underline{U}_{bottom} \tag{4.225}$$

We now write the relative displacements as

$$\delta\underline{U} = [\mathbf{N}_{top}, -\mathbf{N}_{bottom}] \begin{Bmatrix} \underline{U}_{top} \\ \underline{U}_{bottom} \end{Bmatrix} \tag{4.226}$$

Fig (4.8) shows the bottom surface of the element.$\underline{V}_\xi$ and $\underline{V}_\eta$ span the tangential plane at a given point on the surface. $\underline{V}_\xi$ and $\underline{V}_\eta$ are given by

$$\underline{V}_\xi = \begin{Bmatrix} \frac{\partial x}{\partial \xi} \\ \frac{\partial y}{\partial \xi} \\ \frac{\partial z}{\partial \xi} \end{Bmatrix} \qquad \underline{V}_\eta = \begin{Bmatrix} \frac{\partial x}{\partial \eta} \\ \frac{\partial y}{\partial \eta} \\ \frac{\partial z}{\partial \eta} \end{Bmatrix}. \tag{4.227}$$

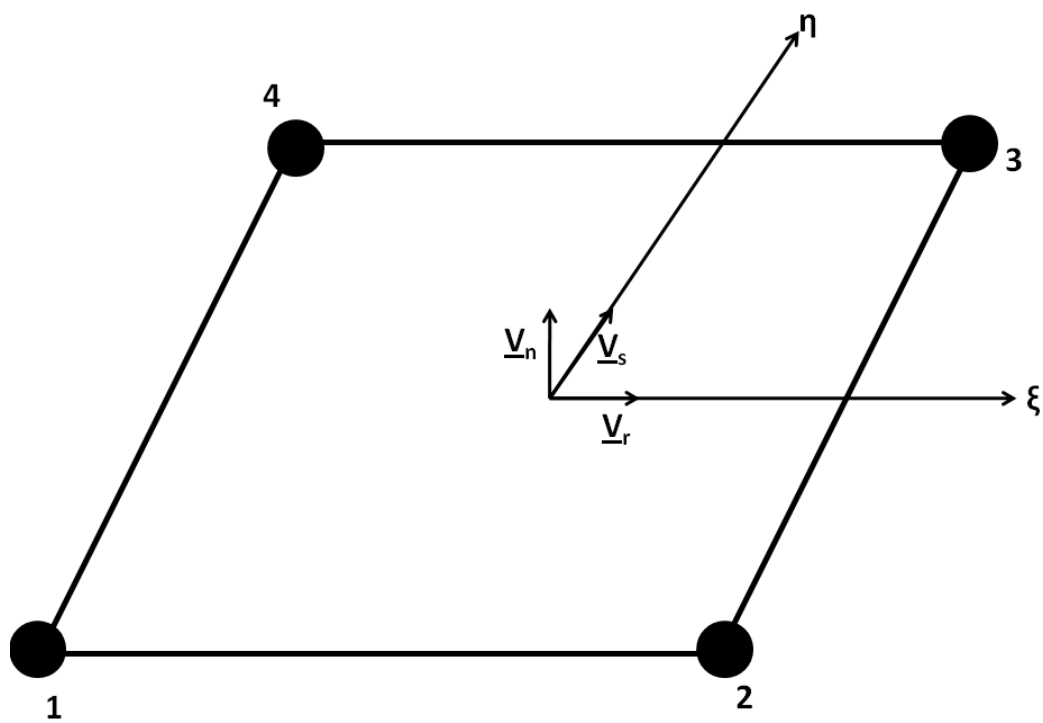

Fig. 4.8. Bottom face of interface element

The unit vectors normal and tangent to the element bottom surface are given by

$$\underline{V}_n = \frac{\underline{V}_\xi \times \underline{V}_\eta}{|\,\underline{V}_\xi\,||\,\underline{V}_\eta\,|}; \tag{4.228}$$

$$\underline{V}_r = \frac{\underline{V}_\xi}{|\,\underline{V}_\xi\,|} \text{ and} \tag{4.229}$$

$$\underline{V}_s = \underline{V}_n \times \underline{V}_r. \tag{4.230}$$

Generally, $\underline{V}_\xi$ and $\underline{V}_\eta$ need not be orthogonal though their cross product is necessarily orthogonal and forms the normal vector out of the surface, $\underline{V}_n$.

Now the relative displacements around the interface are $\underline{V}_r$ and $\underline{V}_s$ in the direction of slip and $\underline{V}_n$ in the direction of separation.

$$\delta\underline{U}\,(n,r,s) = \begin{Bmatrix} u\,(n,r,s) \\ v\,(n,r,s) \\ w\,(n,r,s) \end{Bmatrix}_{top} - \begin{Bmatrix} u\,(n,r,s) \\ v\,(n,r,s) \\ w\,(n,r,s) \end{Bmatrix}_{bottom}. \tag{4.231}$$

$$= \Theta^T[\mathbf{N}_{top}, -\mathbf{N}_{bottom}] \begin{Bmatrix} \underline{U}_{top} \\ \underline{U}_{bottom} \end{Bmatrix} \tag{4.232}$$

where $\Theta^T = [\underline{V}_n, \underline{V}_r, \underline{V}_n]$, the transformation to the normal and tangential directions.

Thus

$$\delta\underline{U}\,(u,r,s) = \Theta^T[\underline{\mathbf{N}}_{top}, -\underline{\mathbf{N}}_{bottom}] \begin{Bmatrix} \underline{U}_{top} \\ \underline{U}_{bottom} \end{Bmatrix} \tag{4.233}$$

$$= \mathbf{B}\underline{U} \tag{4.234}$$

where

$$\mathbf{B} = \Theta^T[\mathbf{N}_{top}, -\mathbf{N}_{bottom}] \qquad \text{and} \qquad \underline{U} = \begin{Bmatrix} \underline{U}_{top} \\ \underline{U}_{bottom} \end{Bmatrix} \tag{4.235}$$

Given that the displacements $\delta\underline{U}\,(n, r, s)$ are assumed equal to those defined earlier, that is,

$$\delta\underline{U} = \begin{Bmatrix} \delta_{v_z} \\ \delta_{v_x} \\ \delta_{v_y} \end{Bmatrix} \tag{4.236}$$

we now have that

$$\underline{\sigma} = \mathbf{C}\delta\underline{U} \tag{4.237}$$

where

$$\mathbf{C} = \begin{bmatrix} k_1 & 0 & 0 \\ 0 & k_2 & 0 \\ 0 & 0 & k_3 \end{bmatrix} = \text{diag}\,(k_1, k_2, k_3) \tag{4.238}$$

In the softening zone, the constitutive equations are given by

$$\sigma_{zz} = (1-d)\,k_1\delta_{v_z} \tag{4.239}$$

$$\tau_{xz} = (1-d)\,k_2\delta_{v_x} \tag{4.240}$$

$$\tau_{yz} = (1-d)\,k_3\delta_{v_y} \tag{4.241}$$

becoming

$$\underline{\sigma} = (\mathbf{I} - \mathbf{D})\,\mathbf{C}\delta\underline{U} \tag{4.242}$$

$$= (1-d)\,\mathbf{CB}\underline{U} \tag{4.243}$$

where

$$\mathbf{D} = \begin{bmatrix} d & 0 & 0 \\ 0 & d & 0 \\ 0 & 0 & d \end{bmatrix} \tag{4.244}$$

$\mathbf{I} =$ the identity matrix

Our task is to determine the displacements $\underline{U}$ of the body and to achieve this, we employ the principle of minimum potential energy which states that for conservative systems, of all the

kinematically admissible displacement fields, those corresponding to the equilibrium equations extremises the total potential energy [CHANDRUPATLA and BELEGUNDU, 1997].

Now the total potential energy π_p [RAO, 2005] of an elastic body is defined as the sum of the total strain energy π and the work done on the body by external loads W_p:

$$\pi_p = \pi + W_p \tag{4.245}$$

Since both terms involve integrals over the volume, we shall replace each by the sum of the integrals over each element so that

$$\sum_{e=1}^{E} \pi_p^{(e)} = \sum_{e=1}^{E} \left(\pi^{(e)} - W_p^{(e)}\right) \tag{4.246}$$

where E is the total number of elements used in the cohesive zone. The strain energy for element Ω^e is then given by

$$\pi^{(e)} = \frac{1}{2}\int_{\Omega^e} \delta_{\underline{U}}^T \cdot \underline{\sigma} dV \tag{4.247}$$

$$= \frac{1}{2}\int_{\Omega^e} \underline{U}^T \mathbf{B}^T \left(\mathbf{I} - \mathbf{D}\right) \mathbf{CB} \underline{U} dV \tag{4.248}$$

Similarly it can be shown that $W_p^{(e)}$ reduces to $-\left(\underline{U}\right)^T \underline{F}$ where $\underline{F}$ refers to the external load in the beam.

Invoking the principle of minimum potential at the element level results in the element equation

$$K^{(e)} \underline{U}^{(e)} = \underline{F}^{(e)} \tag{4.249}$$

where $K^{(e)} = \int_{\Omega^e} \mathbf{B}^T \left(1 - d\right) \mathbf{CB} dV$ is the element stiffness matrix.

The system is then assembled and solved in the traditional way discussed in Chapter 3.

Chapter 5
Delamination case study

In this chapter, we will carry out the delamination simulation of our composite sandwich beam using the MSC software packages, MSC.Marc and MSC.Mentat. For this, we use the cohesive zone modelling technique outlined in the previous chapter. For the pre- and post-processing, we will use MSC.Mentat and use the nonlinear finite element software MSC.Marc to solve the model.

5.1 Pre-processing

To create the model, three 2D regions, which are surfaces corresponding to the two matching facesheets and sandwich core, are defined. These regions are then meshed using plane stress elements, element number 3 from the MSC.Marc element library [MSC.Software, 2007]. These elements are 4-noded planar elements. The element material properties are then introduced by employing the material values defined in Chapter 3. Compared to the 3D interface elements previewed in Chapter 4, we will consider the quadrilateral element defined by nodes 1,2,6,5 and omit the other nodes in the ensuing interface element formulation.

In this study, the interface elements have the same mesh as the core and facesheets. The interface elements have zero thickness and are inserted between the core and the facesheet. No contact modelling is necessary to join the layers of the composite sandwich beam as they will be joined together by the interface elements. The interface elements can

be interpreted as the glue or adhesive bonding the separating layers together but the key difference is that the interface elements have zero thickness.

In creating interface elements, matching boundaries are first defined which will be consequently joined together by the interface elements. The bottom layer is assumed to have a crack of 5mm. For the 190mm beam, there will be a 185mm matching boundary from where the crack can be monitored. The properties of the cohesive zone were obtained from the CSIR and are given as follows

$$G_c = 450\text{N/m} \tag{5.250}$$

where G_c is the critical energy release rate, and

$$T = 10.37\text{MPa} \tag{5.251}$$

where T is the interlaminar shear strength of the composite sandwich beam. The value for $\delta_{v_{\max}}$ is calculated from the equations defined in Chapter 4, as

$$\delta_{v_{\max}} = \frac{2G_c}{T} = 8.679 \times 10^{-5}\text{m} \tag{5.252}$$

For reasons outlined in Chapter 4, the penalty parameter will be set to $1 \times 10^6\text{mm}^{-1}$ so that

$$\delta_{v_{crit}} = \frac{1}{k} = 1 \times 10^{-6}\text{mm} \tag{5.253}$$

Having obtained $\delta_{v_{crit}}$, the material description of the interface behaviour is complete.

The core was meshed by 760×30 elements whilst the facesheets were meshed by 760×2 elements. The reason for the mesh was to have a fine mesh to represent the cohesive but at the same time maintaining the aspect ratio, that is, the ratio of the width to the height of the elements at around 0.5 to 1 to avoid highly distorted elements during the analysis.

As mentioned earlier, an initial crack of 5mm was placed in between the bottom facesheet and the core to monitor delamination growth. A contact body consisting of all the elements was then defined to prevent penetration at the initial crack. The model was then subjected to a four point load by giving two nodes at a quarter the distance from the edge a prescribed displacement and then solving the model in MSC.Marc.

5.2 Results and Discussion

The following diagrams show a graphical output of the delamination analysis of the composite analysis from MSC.Marc and MSC.Mentat. Fig (5.9) is made deliberately larger than the other snapshots to enhance readability.

From the snapshots, it can be seen that the facesheet starts to buckle as the delamination progresses. The damage is confined to the interface between the core and facesheet in which we placed our initial crack. The delamination was studied only as a numerical exercise and as such, no experiments were carried out to validate the above model.

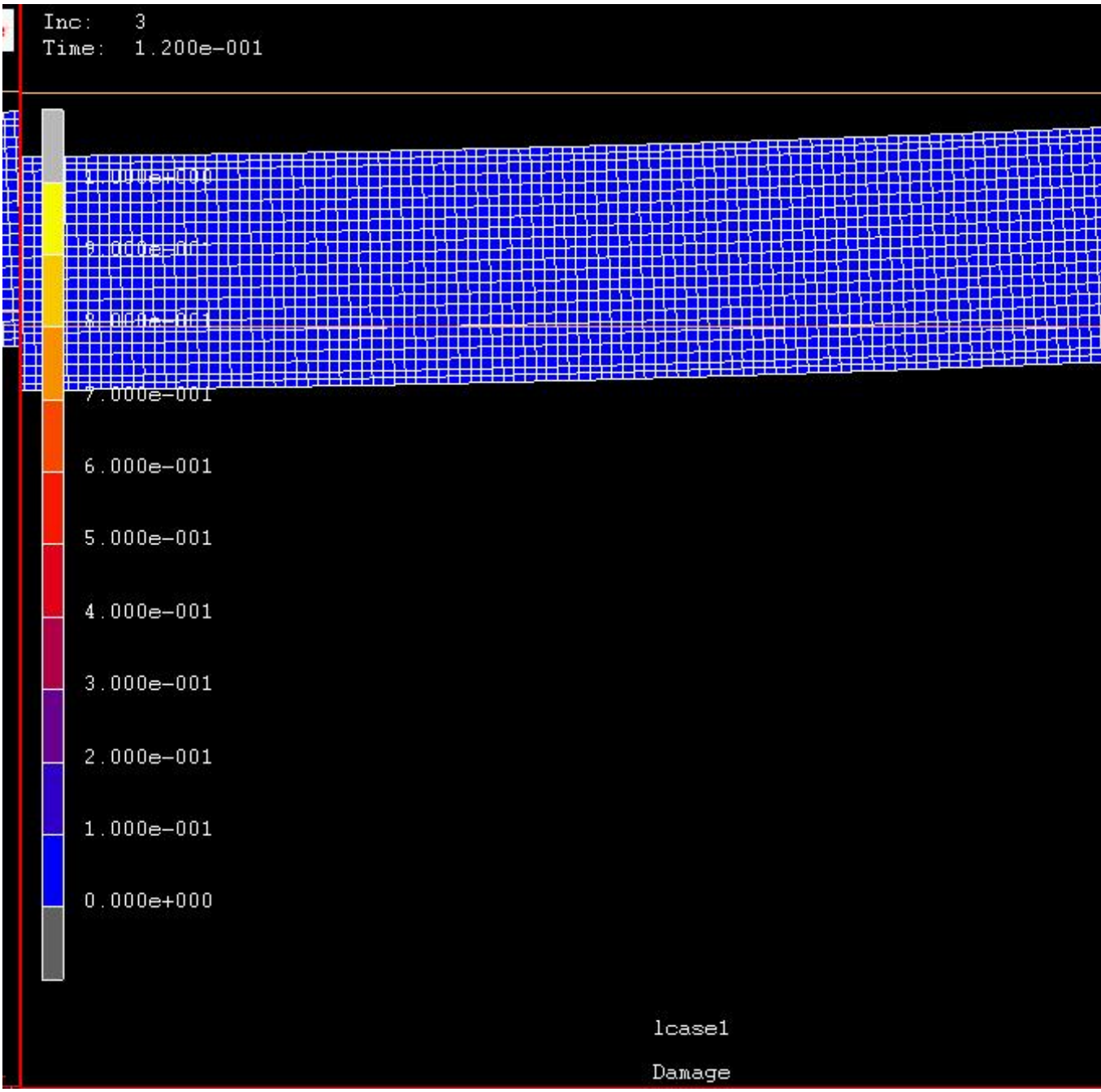

Fig. 5.9. Damage profile after 3/50 increments

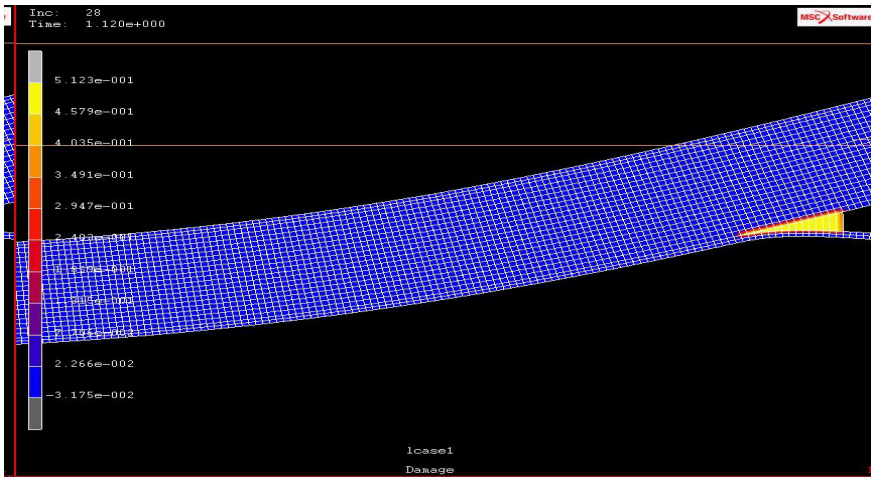

Fig. 5.10. Damage profile after 28/50 increments

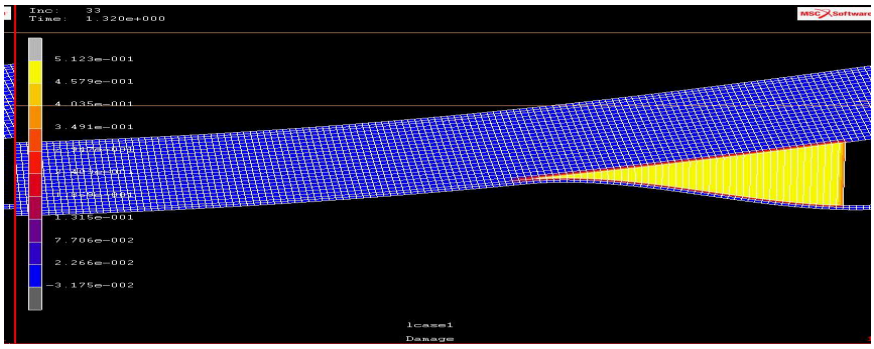

Fig. 5.11. Damage profile after 33/50 increments

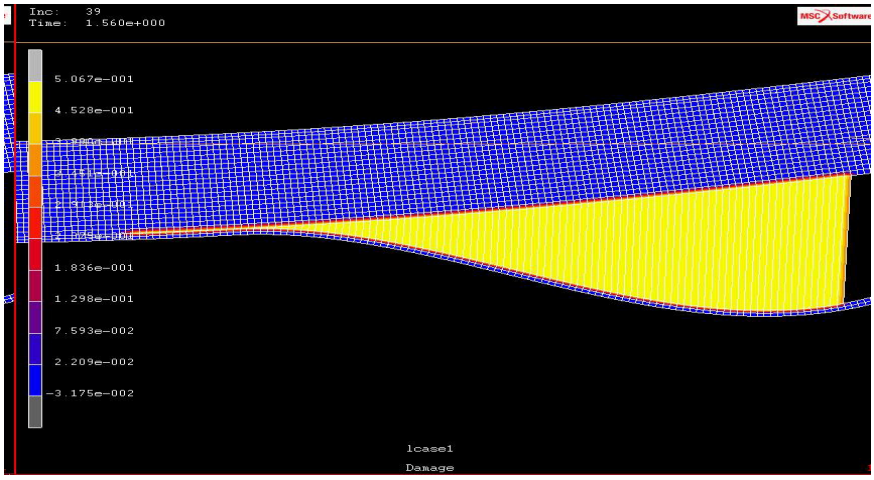

Fig. 5.12. Damage profile after 39/50 increments

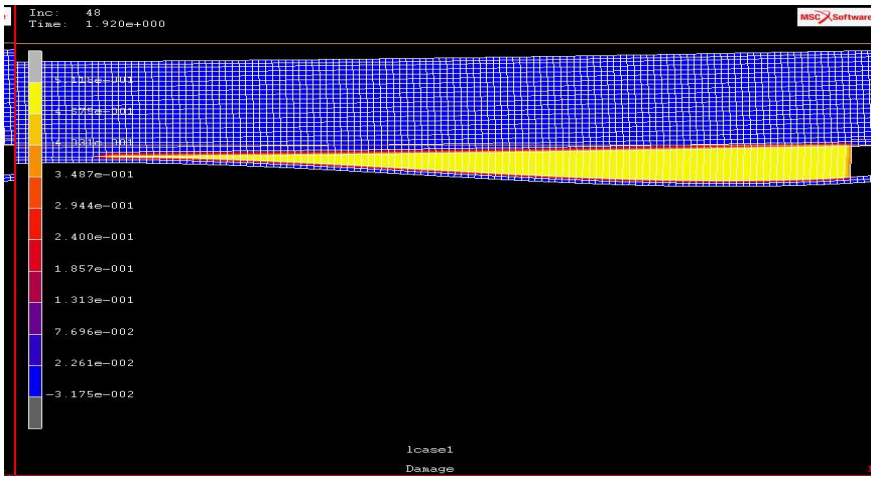

Fig. 5.13. Damage profile after 48/50 increments

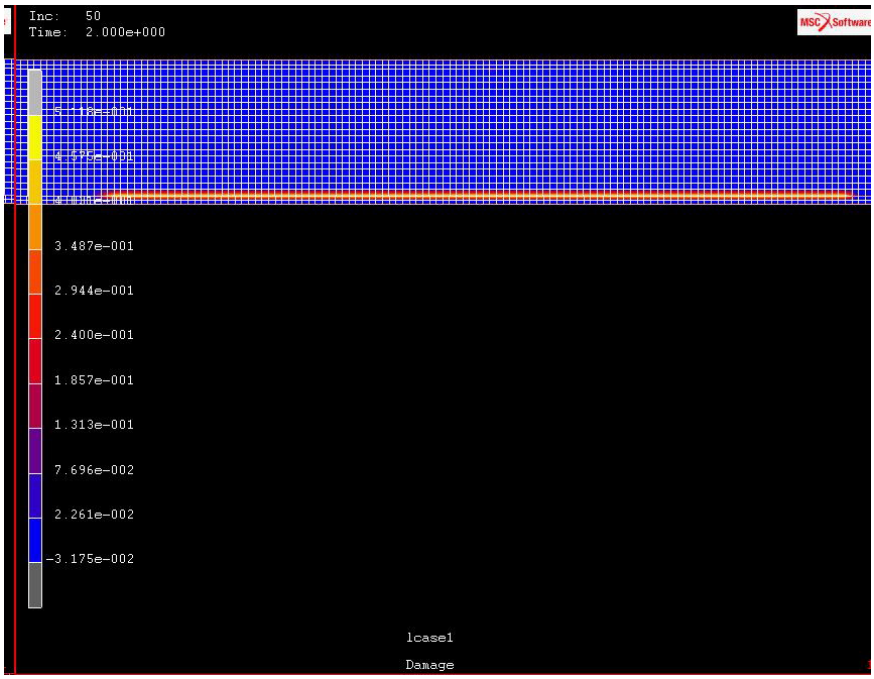

Fig. 5.14. Damage profile after 50/50 increments

Chapter 6
Conclusion and Recommendations for further work

In this dissertation, the bending analysis of a composite sandwich beam has been conducted primarily from a 2D view of the panel. Whilst the panel has a 3D structure, by making certain kinematic assumptions about the beam allows us to reduce the model from 3D to 1D. Bending analysis was done using the Timoshenko beam theory which accepts transverse shear. Instead of simply using the Timoshenko beam theory, we first reviewed the literature to derive a deeper understanding of the derivation of the governing equations by using the principle of virtual work.

The principle of virtual work is a powerful tool from variational mechanics which can be used to derive the equilibrium equations for a linear or nonlinear theory. Derivation of the linear and nonlinear governing equations follows a similar pattern save for the geometric nonlinear term. Solving of the two models was done using a MATLAB code. The linear and nonlinear finite element analysis code gave correct qualitative results. To validate the model, a series of four point bending experiments were carried out at the CSIR using a composite sandwich beam with the same dimensions. The results compared favourably with nonlinear numerical results with increasing variations between numerical and experimental results due to indentation of the composite sandwich beam.

The cohesive zone modelling technique was also reviewed from a 3D viewpoint with a means to understand the delamination mechanics. Delamination consists of delamina-

tion initiation and then delamination propagation once the irreversible damage has set in. Delamination initiation is governed by the Brewer and Lagace Quadratic Stress Criterion whereas delamination growth is governed by fracture mechanics. The delamination model was carried out using the nonlinear software MARC. The results obtained gave a correct qualitative explanation of delamination mechanics.

The model whilst giving some insight into the bending mechanics can be improved by taking into effect the material nonlinearity of the core and facesheet. The Nomex honeycomb core is nonlinear but reasonable results are obtained for small stress and strains.

6.1 Recommendations

- The model can be improved by also including the material nonlinearity of the core and facesheet.
- It may also be beneficial to capture the bending analysis using continuum elements which would update the displacement solution with material position.
- The micro structure of the facesheet may also be modelled to capture the effects of the bending stresses on the natural fibres.

Appendix A
Gaussian Quadrature

Gaussian quadrature points and weights over the interval $[-1, 1]$. m is the order of polynomial which is exactly reproduced by the quadrature scheme.

n	ξ_i	w_i	$m = 2n - 1$
1	0	2	1
2	$\pm\frac{1}{\sqrt{3}}$	1	3
3	0	$8/9$	
	$\pm\sqrt{3/5}$	$5/9$	5
4	$\pm\sqrt{\frac{3-2\sqrt{6/5}}{7}}$	$\frac{1}{2} + \frac{1}{6\sqrt{6/5}}$	
	$\pm\sqrt{\frac{3+2\sqrt{6/5}}{7}}$	$\frac{1}{2} - \frac{1}{6\sqrt{6/5}}$	7

Appendix B
Green strain and infinitesimal strain tensor

The motion of a body in a general continuum [LAI et al., 1993, REDDY, 2008] can be described by a vector equation of the form

$$\mathbf{x} = \mathbf{x}\left(\mathbf{X}, t\right) \quad \text{with} \quad \mathbf{x}\left(\mathbf{X}, t_o\right) = \mathbf{X} \tag{B.1}$$

where $\mathbf{x}$ is the position vector at time t for a particle which was at $\mathbf{X}$ at some reference time t_o. The displacement of a particle which was initially at position $\mathbf{X}$ at reference time t_o to a position $\mathbf{x}$ at time t is given by

$$\mathbf{u}\left(\mathbf{X}, t\right) = \mathbf{x} - \mathbf{X} \tag{B.2}$$

Taking the total derivative of equation $(B.2)$ gives the following after applying the chain rule

$$d\mathbf{x} = d\mathbf{X} + \left(\nabla \mathbf{u}\right) d\mathbf{X} = \mathbf{F} d\mathbf{X} \tag{B.3}$$

where $\mathbf{F}$, the deformation gradient is defined as

$$\mathbf{F} = \mathbf{I} + \nabla \mathbf{u} \tag{B.4}$$

Taking the dot product of $d\mathbf{X}$ with itself and similarly taking the dot product of $d\mathbf{x}$ with itself gives

$$d\mathbf{X} \cdot d\mathbf{X} = \left(dS\right)^2 \tag{B.5}$$

$$d\mathbf{x} \cdot d\mathbf{x} = \left(ds\right)^2 = \mathbf{F} d\mathbf{X} \cdot \mathbf{F} d\mathbf{X} = d\mathbf{X} \cdot \left(\mathbf{F}^T \mathbf{F}\right) \cdot d\mathbf{X} \tag{B.6}$$

From equations $(B.6)$ and $(B.5)$, we have the following

$$(ds)^2 - (dS)^2 = d\mathbf{X}\cdot\left(\mathbf{F}^T\mathbf{F}\right)\cdot d\mathbf{X} - d\mathbf{X}\cdot d\mathbf{X} = \mathbf{2}d\mathbf{X}\cdot\mathbf{E}\cdot d\mathbf{X} \tag{B.7}$$

where $\mathbf{E}$ is called the Green-St Venant strain tensor or better known as the Green strain tensor which is defined as

$$\begin{aligned}
\mathbf{E} &= \frac{1}{2}\left(\mathbf{F}^T\mathbf{F} - \mathbf{I}\right) && \text{(B.8)}\\
&= \frac{1}{2}\left[(\mathbf{I} + \nabla\mathbf{u})^T\cdot(\mathbf{I} + \nabla\mathbf{u}) - \mathbf{I}\right] && \text{(B.9)}\\
&= \frac{1}{2}\left[\nabla\mathbf{u} + (\nabla\mathbf{u})^T + (\nabla\mathbf{u})\cdot(\nabla\mathbf{u})^T\right] && \text{(B.10)}
\end{aligned}$$

In Cartesian coordinate system, the components of $\mathbf{E}$ are given by

$$E_{ij} = \frac{1}{2}\left(\frac{\partial u_i}{\partial X_j} + \frac{\partial u_j}{\partial X_i} + \frac{\partial u_m}{\partial X_i}\frac{\partial u_m}{\partial X_j}\right) \tag{B.11}$$

Now, considering only cases where the components of the displacement vector as well as their partial derivatives, that is, $|\nabla\mathbf{u}| << 1$, $(\nabla\mathbf{u})\cdot(\nabla\mathbf{u})^T$ can be neglected and we get the infinitesimal strain tensor, $\boldsymbol{\varepsilon}$, given by

$$\varepsilon_{ij} = \frac{1}{2}\left(\frac{\partial u_i}{\partial X_j} + \frac{\partial u_j}{\partial X_i}\right) \tag{B.12}$$

References

ANANDJIWALA, R., JOHN, M., WAMBUA, P., CHAPPLE, S., KLEMS, T., DOECKER, M., GOULAIN, M., and ERASMUS, L. (2008). Bio-based structural composite materials for aerospace applications. In *2nd SAIAS Symposium*.

BELYTSCHKO, T., LIU, W., and MORAN, B. (2000). *Nonlinear Finite Elements for Continua and Structures*. John Wiley and Sons, Ltd.

BIRMAN, V. and BERT, C. (2002). On the choice of shear correction in sandwich structures. *Journal of Sandwich Structures and Materials*, 4(1):83–95.

BREWER, J. and LAGACE, P. (1988). Quadratic stress criterion for initiation of delamination. *Journal of Composite Materials*, 22(12):1141–1155.

BUITRAGO, B., SANTIUSTE, C., SANCHEZ-SAEZ, S., BARBERO, E., and NAVARRO, C. (2010). Modelling of composite sandwich structures with honeycomb core subjected to high-velocity impact. In *Fifteenth International Conference on Composite Structures*, volume 92.

CAMANHO, P., DAVILA, C., and de MOURA, M. (2003). Numerical simulation of mixed-mode progressive delamination in composite materials. *Journal of Composite Materials*, 37(16):1415–1424.

CASTANIE, B., BOUVET, C., AMINANDA, Y., BARRAU, J., and THEVENET, P. (2008). Modelling of low-energy/low-velocity impact on nomex honeycomb sandwich structures with metallic skins. *International Journal of Impact Engineering*, 35:620–634.

CHANDRUPATLA, T. and BELEGUNDU, A. (1997). *Introduction to Finite Element in Engineering*, volume 2. Prentice-Hall International.

CHEN, H. and BAI, R. (2002). Postbuckling behaviour of face/core debonded composite sandwich plate considering matrix crack and contact effect. *Journal of Composite Structures*, 57:305–313.

CLOUGH, R. (1960). The finite element method in plane stress analysis. In *Proceedings of the Second ASCE Conference on Electronic Computation, Pittsburgh*.

CUI, W. and WISNOM, M. (1993). A combined stress-based and fracture-mechanics-based model for predicting delamination in composites. *Journal of Composites Part A: Applied Science and Manufacturing*, 24(6):467–474.

DAVILA, C., CAMANHO, P., and de MOURA, M. (2001). Mixed-mode decohesion elements for analysis of progressive delamination. In *Structural Dynamics and Materials Conference*, volume 42.

de MOURA, M., GONCALVES, J., MARQUES, A., and de CASTRO, P. (1997). Modeling compression failure after low velocity impact on laminated composites using interface elements. *Journal of Composite Materials*, 31(15):1462–1479.

de MOURA, M., GONCALVES, J., MARQUES, A. M., and de CASTRO, P. (2000). Prediction of compressive strength of carbon-epoxy laminates containing delamination by using a mixed-mode damage model. *Journal of Composite Structures*, 50:151–157.

FOO, C., CHAI, G., and SEAH, L. (2008). A model to predict low-velocity impact response and damage in sandwich composites. *Journal of Composites Science and Technology*, 68:1348–1356.

GDOUTOS, E. and DANIEL, I. (2008). Nonlinear stress and deformation behaviour of composite sandwich beams. *Journal of Applied Mechanics and Materials*, 13-14:91–98.

GIBSON, R. (2007). *Principles of Composite Material Mechanics*. CRC Press.

GOCKENBACH, M. (2006). *Understanding and Implementing the Finite Element Method*. Society for Industrial and Applied Mathematics.

GONCALVES, J., de MOURA, M., de CASTRO, P., and MARQUES, A. (2000). Interface element including point-to-surface constraints for three-dimensional problems with damage propagation. *Journal of Composites Part A: Applied Science and Manufacturing*, 17(1):28–47.

HJELMSTAD, K. (2005). *Fundamentals of Structural Mechanics*. Springer.

HORRIGAN, D., AITKEN, R., and MOLTSCHANIWSKYI, G. (2000). Modelling of crushing due to impact in honeycomb sandwiches. *Journal of Sandwich Structures and Materials*, 2(2):131–151.

IRWIN, G. (1958). *Handbuch der Physik*, volume 6. Springer.

IVANEZ, I., SANTIUSTE, C., and SANCHEZ-SAEZ, S. (2010). Fem analysis of dynamic flexural behaviour of composite sandwich beams with foam core. *Composite Structures*, 92:2285–2291.

JOHNSON, A. and HOLZAPFEL, M. (2003). Modelling soft body impact on composite structures. *Composite Structures*, 61(1-2):103–113.

KRUEGER, R. (2002). The virtual crack closure technique: history, approach and applications. Technical Report NASA/CR-2002-211628, NASA.

KWON, Y. and BANG, H. (1997). *The Finite Element Method Using MATLAB*. CRC Press.

LACY, T. and HWANG, Y. (2003). Numerical modelling of impact-damaged sandwich composites subjected to compression-after-impact loading. *Journal of Composite Structures*, 61(1-2):115–128.

LAI, W., RUBIN, D., and KREMPL, E. (1993). *Introduction to Continuum Mechanics*. Pergamon Press.

LUO, Q. and TONG, L. (2009). Energy release rates for interlaminar delamination in laminates considering transverse shear effects. *Journal of Composite Structures*, 89(2):235–244.

MADABHUSI-RAMAN, P. and DAVALOS, J. (1996). Static shear correction factor for laminated rectangular beams. *Journal of Composites: Part B*, 27B(3-4):285–293.

MEO, M., MORRIS, A., VIGNJEVIC, R., and MARENGO, G. (2003). Numerical simulations of low-velocity impact on an aircraft sandwich panel. *Composite Structures*, 62(3-4):353–360.

MEO, M. and THIEULOT, E. (2005). Delamination modelling in a double cantlilever beam. *Journal of Composite Structures*, 71(3-4):429–434.

MI, Y., CRISFIELD, M., DAVIES, G., and HELLWEG, H. (1998). Progressive delamination using interface elements. *Journal of Composite Materials*, 32(14):1246–1272.

MSC.Software (2007). *Marc and Mentat 2007 r1*. MSC.Software Corporation.

MURA, T. and KOYA, T. (1992). *Variational Methods in Mechanics*. Oxford University Press.

NEEDLEMAN, A. (1987). A continuum model for void nucleation by inclusion debonding. *Journal of Applied Mechanics*, 54(3):525–531.

PALAZOTTO, A., HERUP, E., and GUMMANDI, L. (2000). Finite element analysis of low-velocity impact on composite sandwich plates. *Composite Materials*, 49:209–227.

RAMANTANI, D., CAMPILHO, R., and de MOURA, M. (2010). Stress and failure abalysis of repaired sandwich composite beams using a cohesive damage model. *Journal of Sandwich Structures and Materials*, 12:369–390.

RAO, S. (2005). *The Finite Element Method in Engineering*. Elsevier Butter-Heinemann.

REDDY, J. (1993). *An introduction to the finite element method*. McGraw-Hill, Inc.

REDDY, J. (2004). *Mechanics of Laminated Composite Plates and Shells: Theory and Analysis*. CRC Press.

REDDY, J. (2008). *An Introduction to Continuum Mechanics*. Cambridge University Press.

REEDY, E., MELLO, F., and GUESS, T. (1997). Modeling the initiation and growth of delaminations in composite structures. *Journal of Composite Structures*, 31(8):812–831.

SCHELLEKENS, J. and de BORST, R. (1991). Numerical simulation of free edge delamination in graphite-epoxy lamintes under uniaxial tension. In *Proceedings of the 6th International Conference on Composite Structures*, pages 647–657.

SKAWINSKI, O., BINETRUY, C., KRAWCZAK, P., GRANDO, J., BONNEAU, E., SCANZI, J.-M., and HILAIRE, B. (2004). All-thermoplastic composite sandwich panels - part ii: Modelling of bending behaviour. *Journal of Sandwich Structures and Materials*, 6(5):423–446.

TESSLER, A., SCIUVA, M. D., and GHERLONE, M. (2009). A refined zigzag beam theory for composite and sandwich beams. *Journal of Composite Materials*, 43(9):1051–1081.

TIMOSHENKO, S. (1921). On the correction for shear of the differential equation for transverse vibrations of prismatic bars. *Philosophical Magazine Series 6*, 41(245):744–746.

TVERGAARD, V. and HUTCHINSON, J. W. (1992). The relation between crack growth resistance and fracture process parameters in elastic-plastic solids. *Journal of the Mechanics and Physics of Solids*, 40(6):1377–1397.

WHITNEY, J. and BROWNING, C. (1985). On short-beam shear tests for composite materials. *Journal of Experimental Mechanics*, 25(3):294–300.

WIMMER, G., SCHUECKER, C., and PETTERMANN, H. (2009). Numerical simulation of delamination onset and growth in laminated composite components - a combination

of strength criterion and fracture mechanics. *Journal of Composites Part B: Engineering*, 40(2):158–165.

XU, X. and NEEDLEMAN, A. (1994). Numerical simulations of fast crack growth in brittle solids. *Journal of the Mechanics and Physics of Solids*, 42(9):1397–1434.

ZIENKIEWICZ, O. and TAYLOR, R. (2000). *The Finite Element Method*. Butterworth-Heinemann.

ZOU, Z., REID, S., and LI, S. (2003). A continuum damage model for delaminations in laminated composites. *Journal of the Mechanics and Physics of Solids*, 51(2):333–356.

ZOU, Z., REID, S., LI, S., and SODEN, P. (2002). Modeling interlaminar and intralaminar damage in filament-wound pipes under quasi-static indentation. *Journal of Composite Materials*, 36(4):477–499.